

Porous 3D Polymers for High Pressure Methane Storage and Carbon Dioxide Capture

S. Bracco, D. Piga, I. Bassanetti, J. Perego, A. Comotti,* and P. Sozzani*

Department of Material Science, University of Milano Bicocca, via R.Cozzi 55, 20125
Milano, Italy

Email: angiolina.comotti@mater.unimib.it; piero.sozzani@mater.unimib.it

Table of Contents

1. Experimental Part

Table S1: Molar ratios of reagents for Friedel Craft Alkylation Reaction

Table S2: Molar ratios of reagents for Yamamoto-type Reaction

Elemental analysis

Tables S3-S4: X-ray fluorescence analysis

Details about collection of CH₄ adsorption isotherms at high pressure

2. Thermogravimetric analysis TGA

Figures S1-S13: TGA runs

3. FT-IR Spectroscopy

Figures S14-S23: FT IR spectra of porous polymers

4. Solid State NMR

Figure S24-S25: ¹³C CP MAS NMR of CBZ2 and SPBF

Tables S5-S13: ¹³C chemical shifts of porous polymers

Figure S26: 2D ¹H-¹³C HETCOR NMR of CBZ2 and PORP

5. N₂ Adsorption Isotherms and Pore size distribution

Figures S27-S30: N₂ adsorption isotherms of porous polymers

Figures S31,S32: Pore size distribution by NLDFT model

Figure S33: N₂ adsorption isotherms before and after pressure treatment

6. CH₄ Adsorption Isotherms and Isosteric Heat of Adsorption

Figure S34: cycles of CH₄ adsorption isotherms up to 180 bar

Figure S35: CH₄ adsorption/desorption isotherms of TRIP up to 180 bar

Figures S36,S37: CH₄ isotherms of TRIP and PORP up to 180 bar and 273K

Table S14: Amounts of CH₄ adsorbed at 298K up to 180 bar

Figures S38-S42: Comparison of CH₄ isotherms collected at 273K and 298K

Figure S43: CH₄ heat of adsorption

7. CO₂ Adsorption Isotherms and Isosteric Heat of Adsorption

Figure S44: CO₂ isotherms collected at 273K

Table S15: Amounts of CO₂ adsorbed at 298K and 273K up to 10 bar

Figures S45-S46: CO₂ isotherms collected at 273K and 298K of PAF1 and PAFPORP

Figure S47: CO₂ isosteric heat of adsorption

8. CO₂/N₂ Selectivity

Figure S48: CO₂/N₂ selectivity at 273K and 298K calculated by IAST theory

9. Powder X-ray diffraction PXRD

Figure S49: Powder X-ray diffraction profiles of porous polymers

1. Experimental Part

Table S1. Stoichiometric ratio of the reagents for the Friedel-Crafts alkylation reaction with distinct monomers.

Sample	Monomer	FDA	FeCl ₃	Stoichiometric ratios Mon:FDA:FeCl ₃	1,2-dichloroethane
TRIP	1 g	2.1 ml	3.83 g	1:6:6	20 ml
CBZCH2	1 g	1.5 ml	2.68 g	1:8:8	20 ml
HPSiO ₂	1 g	1.8 ml	3.27 g	1:12:12	20 ml
HPPh	1 g	2.0 ml	3.64 g	1:12:12	20 ml
RUB	1 g	1.3 ml	2.44 g	1:8:8	20 ml
STIL	1 g	2.0 ml	3.60 g	1:4:4	20 ml
HPSiSi	1 g	2.0 ml	3.75 g	1:12:12	20 ml
SPBF	1 g	2.2 ml	4.10 g	1:8:8	20 ml

Table S2. Stoichiometric ratio of the reagents for the Yamamoto-type reaction with distinct monomers.

Sample	Monomer	Ni(COD) ₂	COD	2,2'-bipyridyl	THF	DMF
CBZ1	760 mg	1.2 g	1 ml	1 g	300 ml	200 ml
CBZ2	670 mg	2.0 g	1 ml	1 g	200 ml	200 ml
PORP	800 mg	1.2 g	1 ml	1 g	300 ml	200 ml
PAF1	700 mg	2.0 g	1 ml	1 g	160 ml	180 ml
PAFPOR	370 mg TFM 135 mg PORF	1.0 g	0.5 ml	0.5 g	120 ml	180 ml

Elemental Analysis. TRIP: H 5.35, C 83.73; CBZCH2: H 4.67, C 82.31, N 4.56; HPSiO₂: H 4.33, C 64.34; PORP: C 76.85, H 3.82, N 8.13; CBZ2: H 4.42, C 86.51, N 6.06; PAFPORP: H 3.63, C 74.55, N 7.01.

Synthesis of HKUST-1. The Cu(NO₃)₂•2H₂O (2.4 g, 10.3 mmol, purity 98%) was dissolved in H₂O (30 ml), and 1,3,5,-benzenetricarboxylic acid (0.68 g, 3.2 mmol, purity 98%) was dissolved in ethanol (30 ml). The two solution were combined in a 250 ml one-neck round-bottom flask. DMF (2 ml) was added, and the flask was sealed with a rubber septum. The reaction mixture was heated at 80 °C for 24 h under stirring. The resulting light blue compound was filtered and washed with H₂O and ethanol. The product was further suspended in ethanol at 55 °C for 12 h. The ethanol was removed, fresh ethanol was added, and the suspension was again heated at 55 °C for 12 h. The final product was collected by filtration and activated by heating at 150 °C under vacuum for 4 h.

X-ray Fluorescence Analysis. X-ray fluorescence measurements were performed with an EDXRF Spectrometer Epsilon 3 (Panalytical), equipped with an Rh tube with 50 μ m thin window (max. 50 kV, 3 mA, 2W), a large area SDD detector cooled with a two-stage Peltier, energy resolution of about 145 eV at 5.9 keV. A flexible voltage (5, 9, 12, 20 and 50 kV) with different filters have been used: none, Cu 300 μ m, Cu 500 μ m, Al 50 μ m, Al 200 μ m, Ti 7 μ m and Ag 100 μ m.

Table S3. X-ray fluorescence analysis for Yamamoto-type reaction (Ni%).

Sample	Ni (%)
PAF1	0.027
CBZ1	0.045
CBZ2	0.260

Table S4. X-ray fluorescence analysis for Friedel Craft reaction (Fe%).

Sample	Fe(%)
SPBF	0.126
STIL	0.252
RUB	0.077
HPPh	0.115
CBZCH2	0.164
HPSiO2	0.130
HPSiSi	0.062
TRIP	0.116

Collection of Methane Isotherms (additional information). Methane sorption measurements at high pressure were performed using a Micromeritics High Pressure Volumetric Apparatus (HPAV II), equipped with a pressure-booster compressor. The booster allows the compression of gas from the gas cylinder up to 200 bar. The samples were loaded in a 10ml-steel jar and connected to the instrument by a VCR connection with a 10 µm seal-frit gasket to avoid sample dispersion into the manifold volume. The temperature was controlled using a Julabo F12-ED refrigerated/heating circulator connected with the HPVA circulation Dewar. The free-space volume was measured with helium just before the first run and then inserted manually during experiment elaboration. To avoid errors due to sample contamination between the de-gassing and the measurement stage, sample mass was measured after the analysis. After the experiment, a blank-correction is applied to the isotherm. The blank experiment is obtained by a point-by-point method on five cycles performed with the empty jar.

The as-obtained isotherms are “excess” isotherms, i.e. the excess gas amount that is “adsorbed” by the sample due to their active pore-surfaces. Over 10 bar, the gas density rises above the ideal gas range and this was taken into account in the elaboration. To obtain the “total” absorbed amount (n_{tot}) we considered the total pore volume of the sample (V_p) and methane density ($\rho(P)$) following the relationship: $n_{tot}(P)=n_{ex}(P)+V_p*\rho(P)$. Density values were taken by REFPROP software of NIST database. The volumetric uptake expressed as the volume of the ideal gas over the volume occupied by the same amount at a certain pressure was measured as follows $V/V=(V/g)*[1/(V_p+1/d)]$ where d corresponds to the density of the host walls, as measured by He picnometry.

2. Thermogravimetric analysis TGA

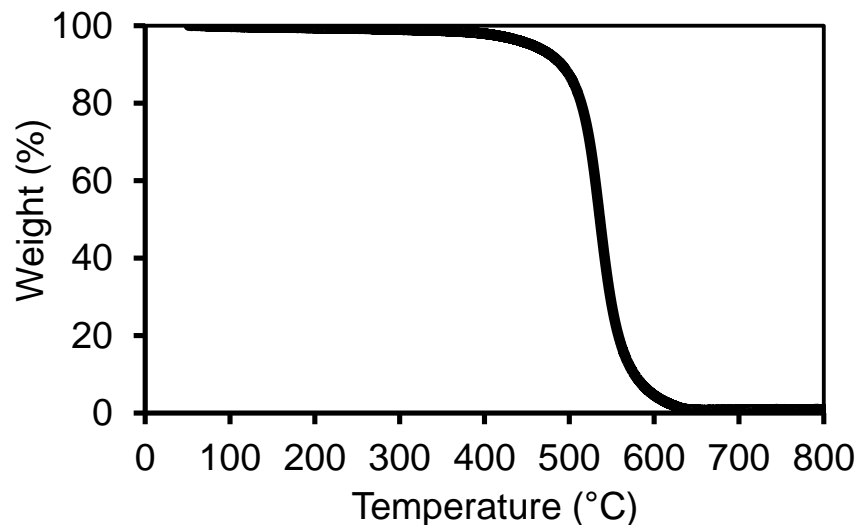


Figure S1. Thermogravimetric analysis of CBZ1 sample performed in air.

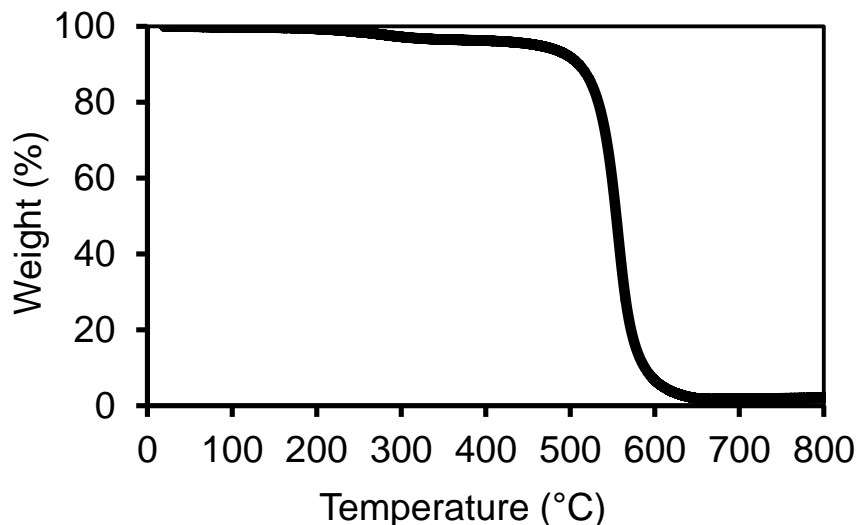


Figure S2. Thermogravimetric analysis of CBZ2 sample performed in air.

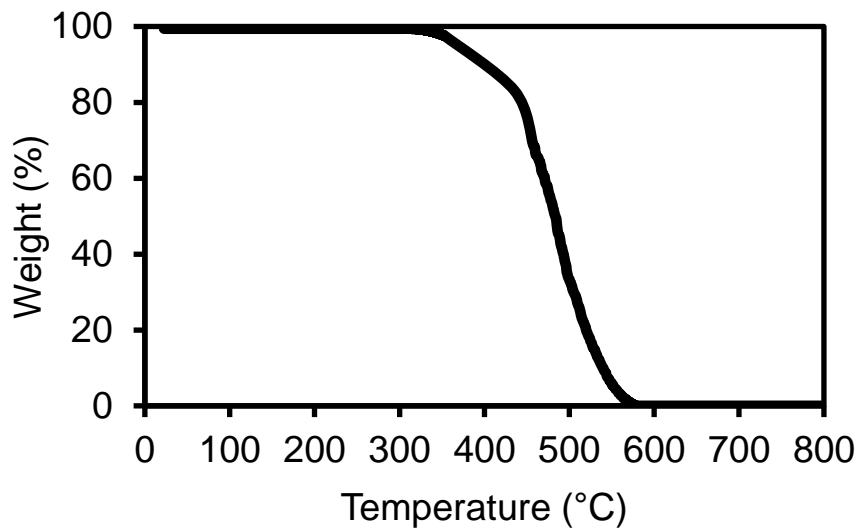


Figure S3. Thermogravimetric analysis of TRIP sample performed in air.

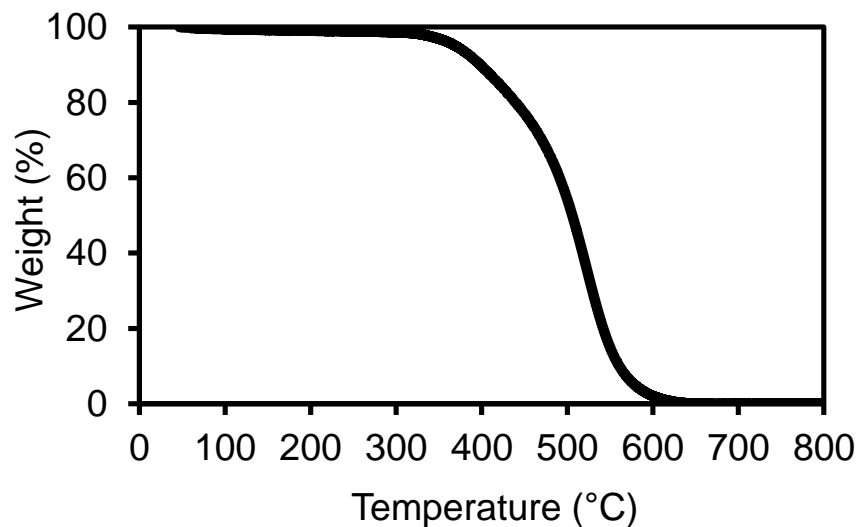


Figure S4. Thermogravimetric analysis of CBZCH₂ sample performed in air.

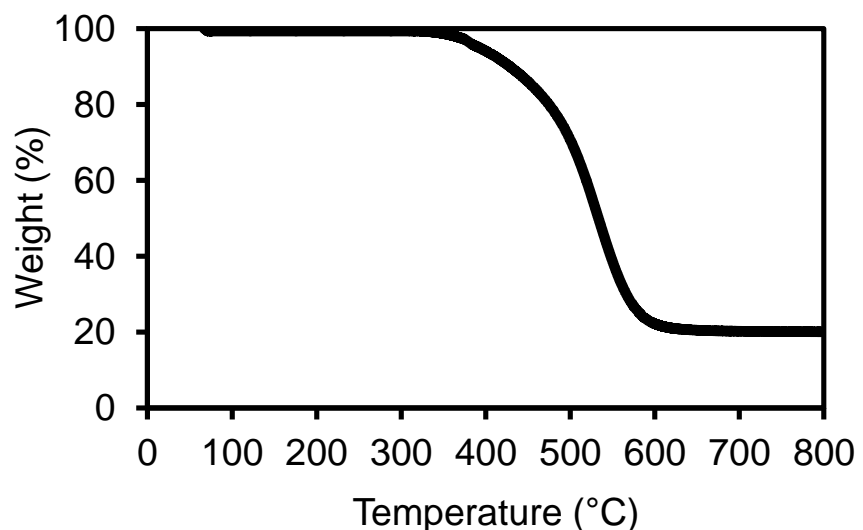


Figure S5. Thermogravimetric analysis of HPSiO₂ sample performed in air.

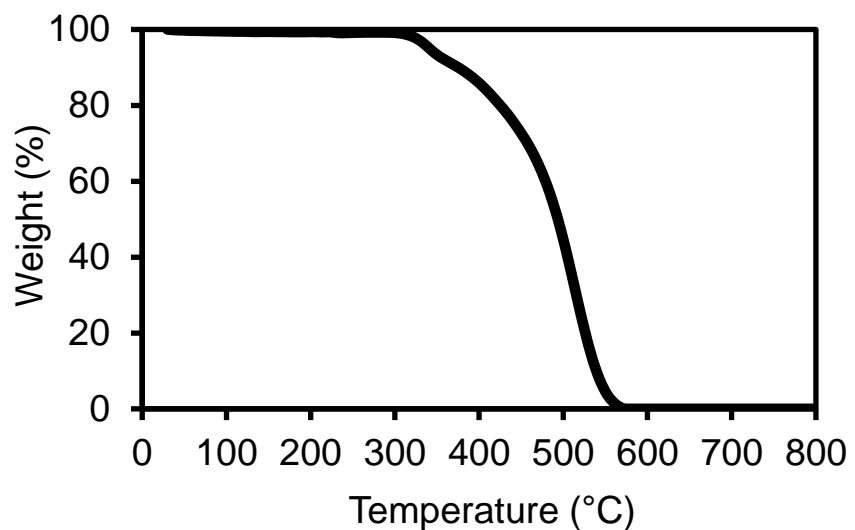


Figure S6. Thermogravimetric analysis of HPPh sample performed in air.

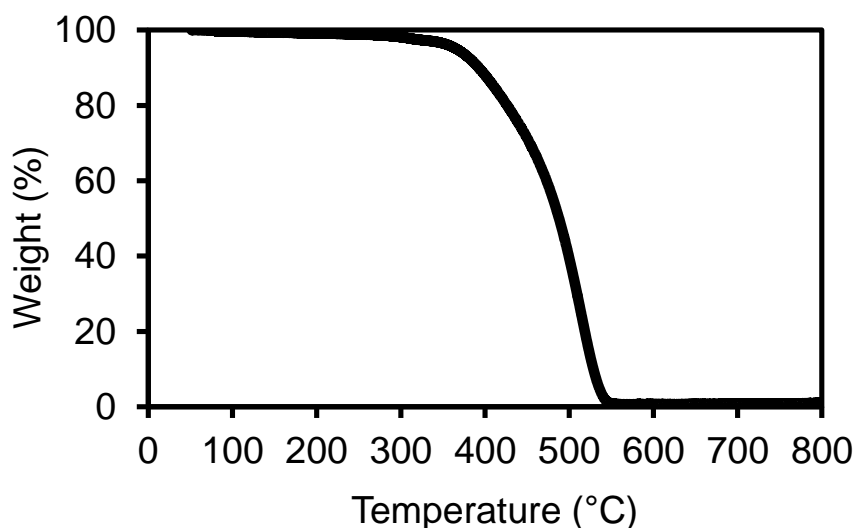


Figure S7. Thermogravimetric analysis of RUB sample performed in air.

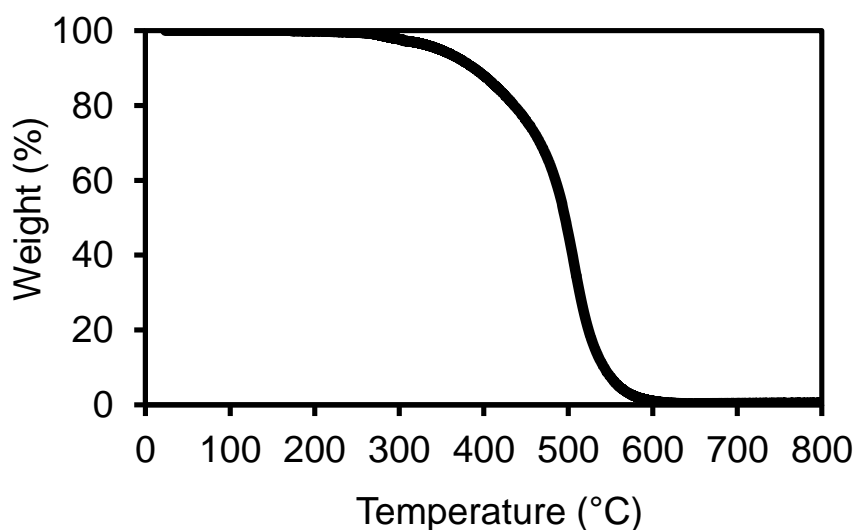


Figure S8. Thermogravimetric analysis of STIL sample performed in air.

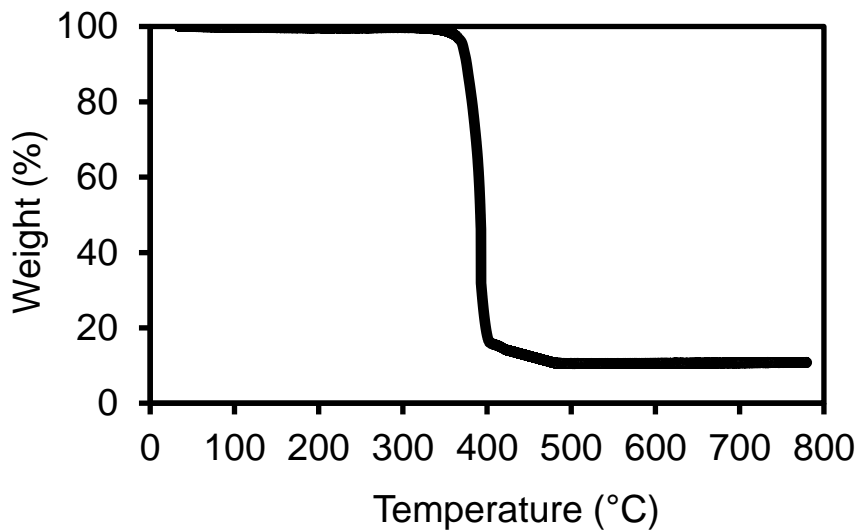


Figure S9. Thermogravimetric analysis of PORP sample performed in air.

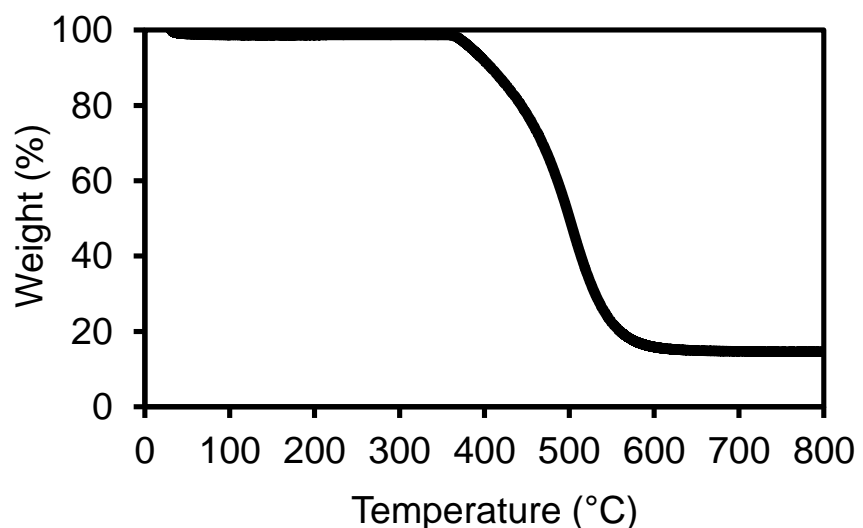


Figure S10. Thermogravimetric analysis of HPSiSi sample performed in air.

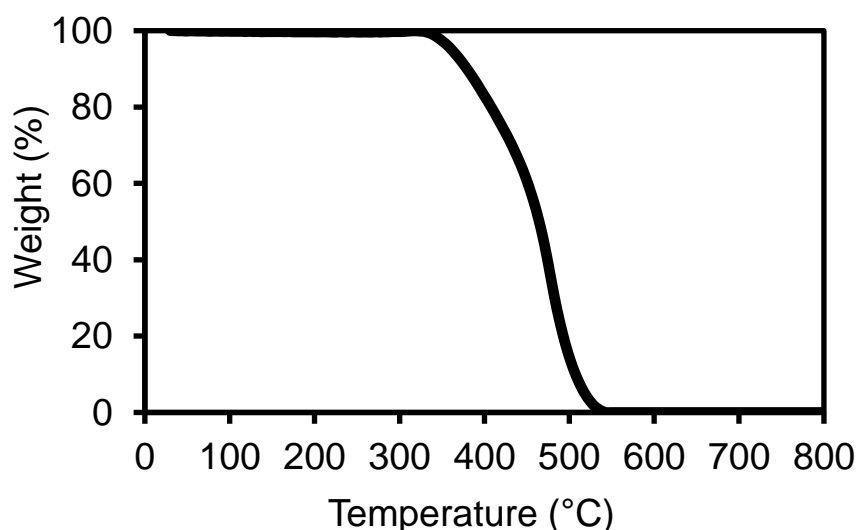


Figure S11. Thermogravimetric analysis of SPBF sample performed in air.

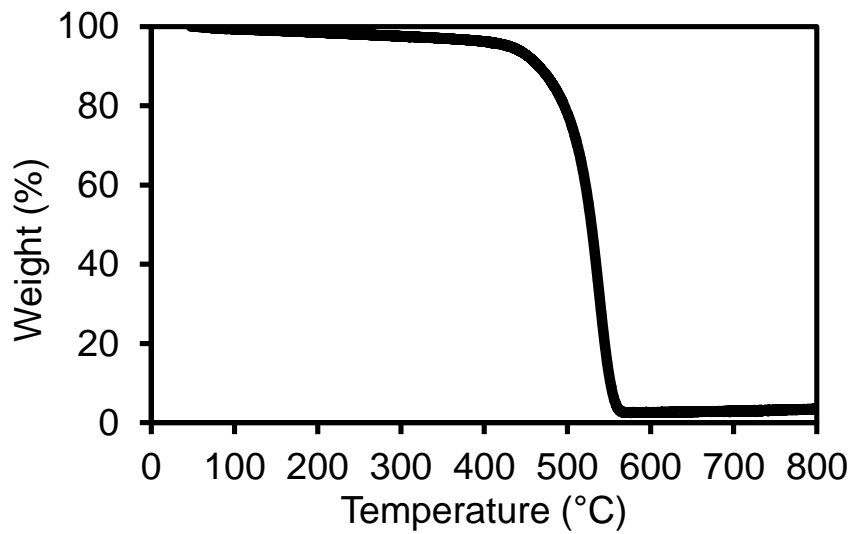


Figure S12. Thermogravimetric analysis of PAF-1 sample performed in air.

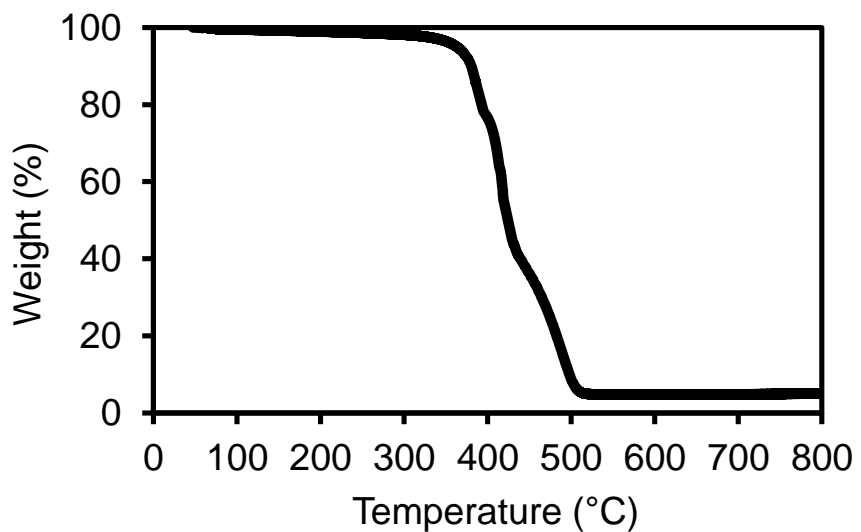


Figure S13. Thermogravimetric analysis of PAFPORF sample performed in air.

3. FT-IR Spectroscopy

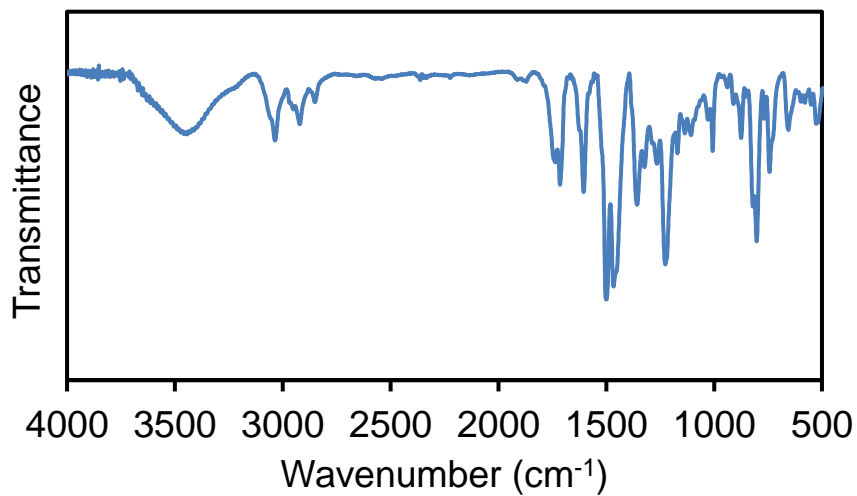


Figure S14. FTIR spectrum of CBZ1 porous polymer.

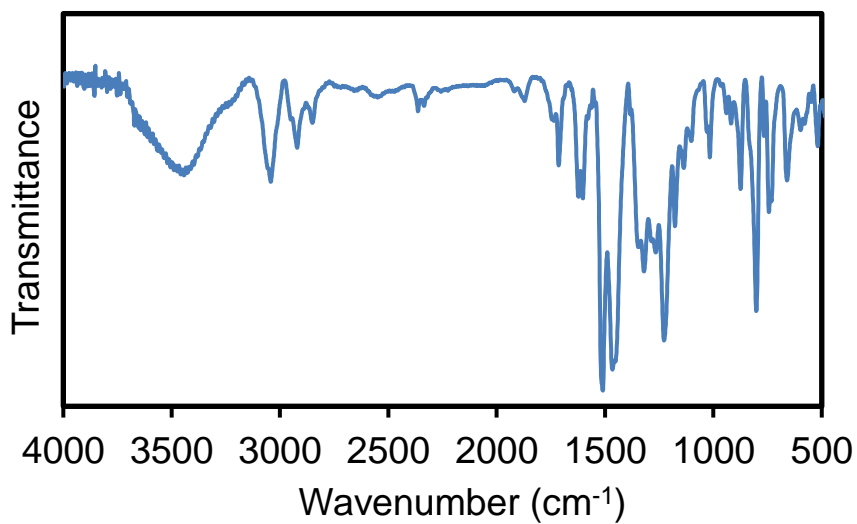


Figure S15. FTIR spectrum of CBZ2 porous polymer.

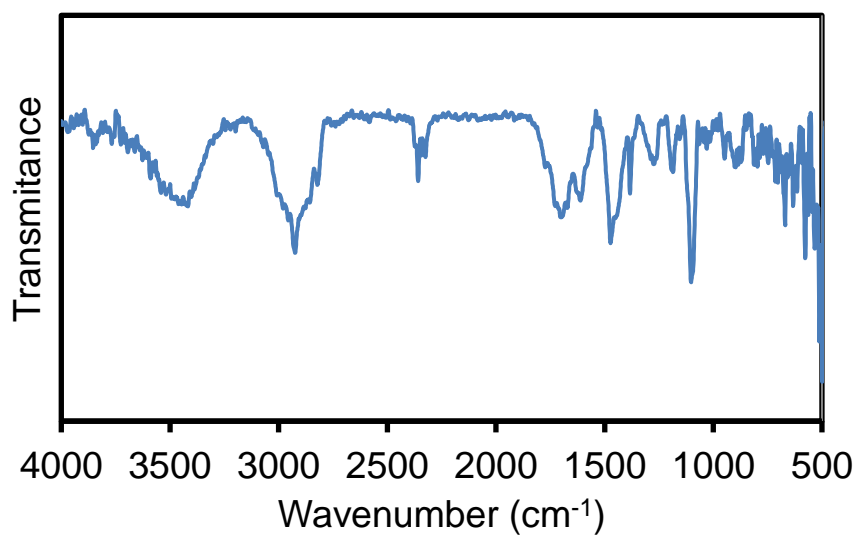


Figure S16. FTIR spectrum of TRIP porous polymer.

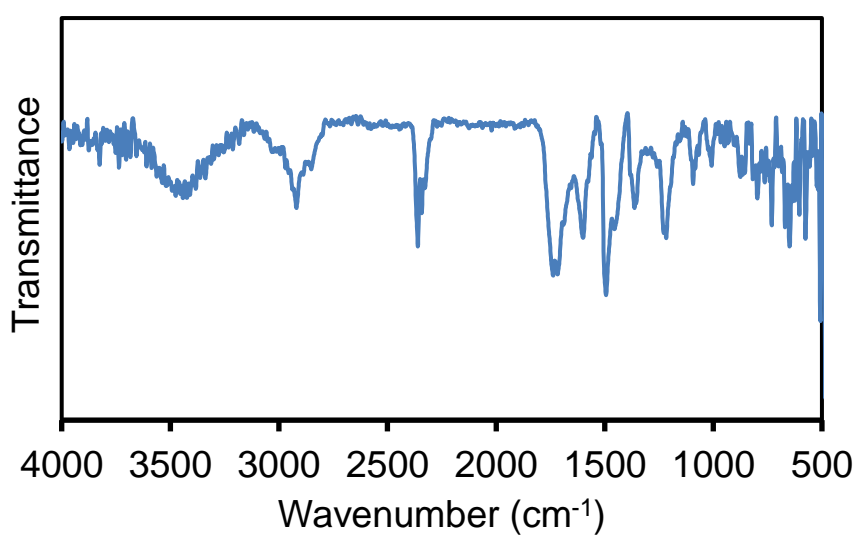


Figure S17. FTIR spectrum of CBZCH₂ porous polymer.

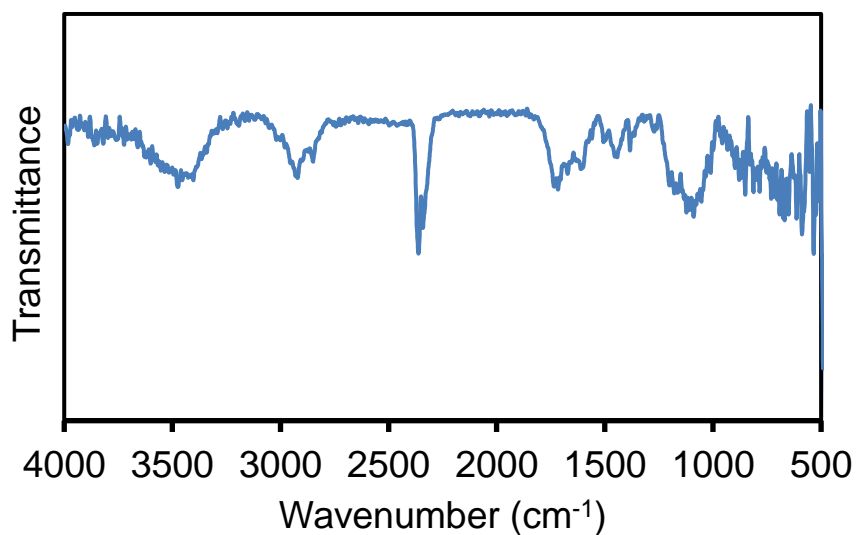


Figure S18. FTIR spectrum of HPSiO₂ porous polymer.

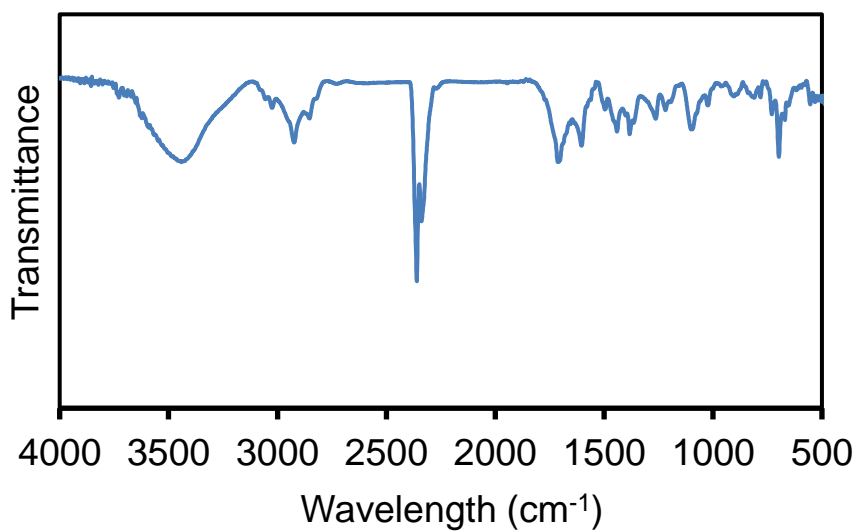


Figure S19. FTIR spectrum of HPPh porous polymer.

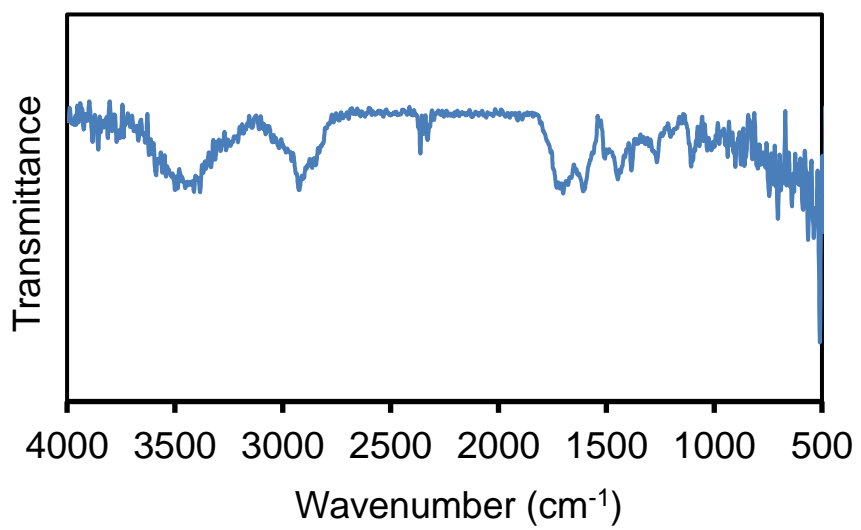


Figure S20. FTIR spectrum of STIL porous polymer.

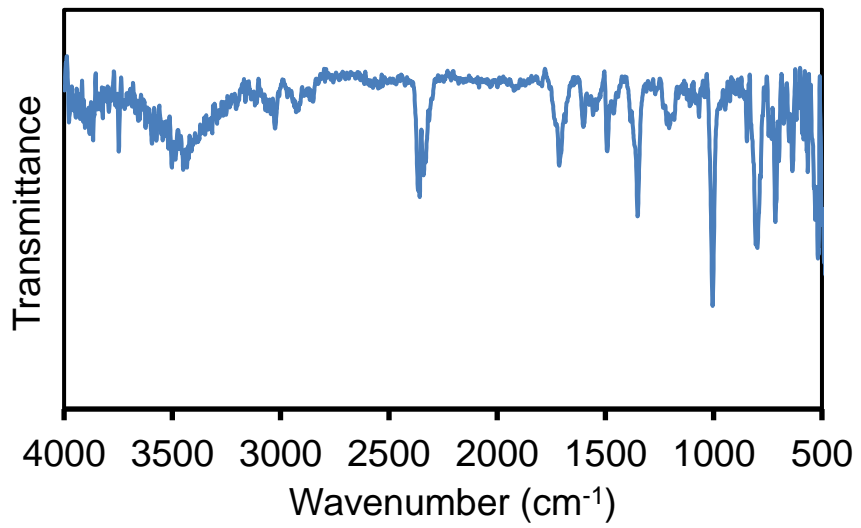


Figure S21. FTIR spectrum of PORP porous polymer.

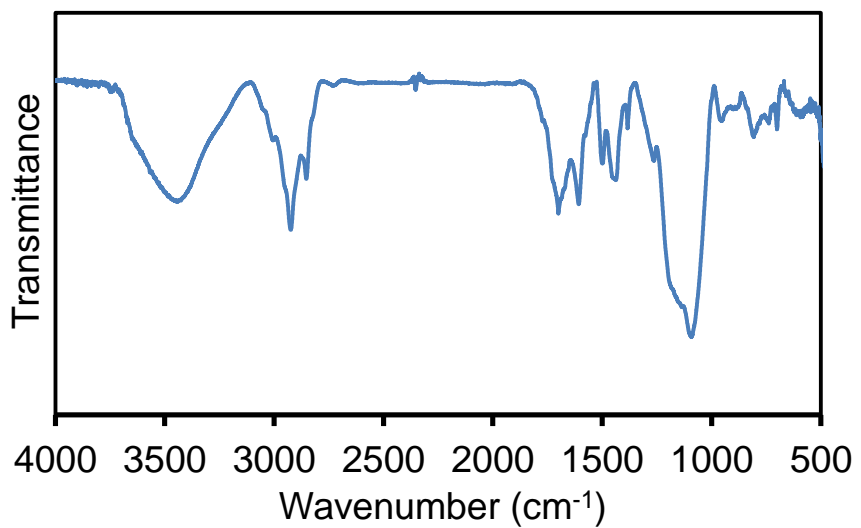


Figure S22. FTIR spectrum of HPSiSi.

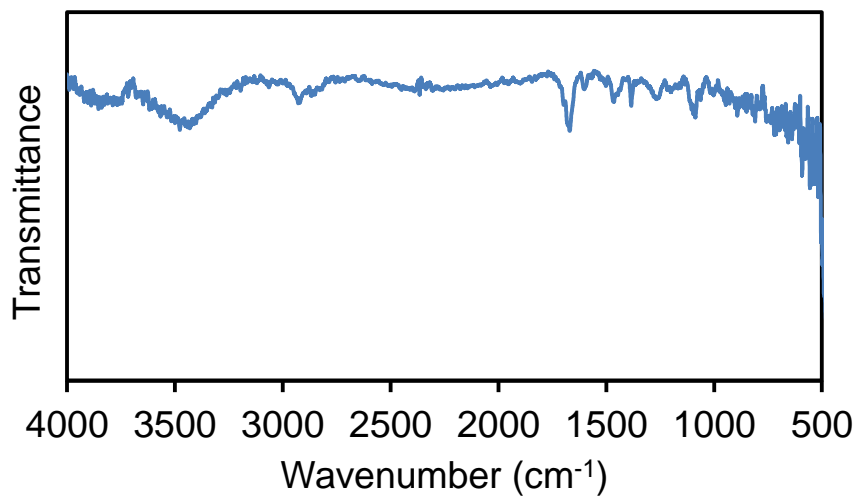


Figure S23. FTIR spectrum of RUB.

4. Solid State NMR

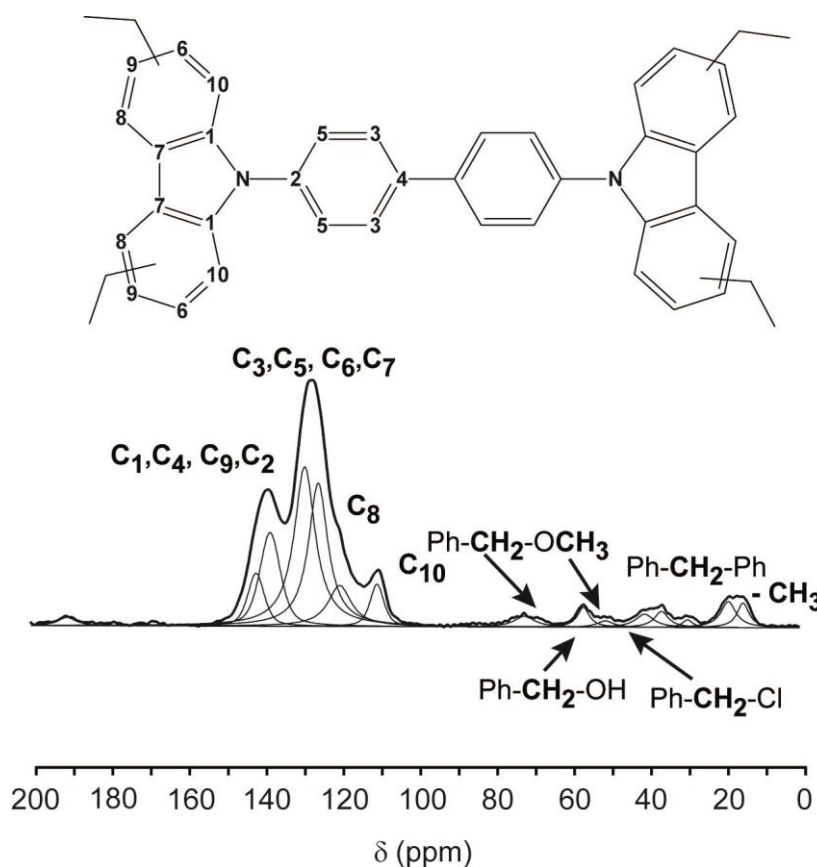


Figure S24. ^{13}C CP MAS OF CBZCH₂ porous polymer.

Table S5. ^{13}C Chemical shifts of CBZCH₂ porous polymer.

CBZCH ₂	
Assignment	δ (ppm)
$\text{C}_1; \text{C}_4; \text{C}_9; \text{C}_2$	141.25/137.62
$\text{C}_3; \text{C}_5; \text{C}_6; \text{C}_7$	128.61/125.10
C_8	119.52
C_{10}	109.82
$\text{Ph}-\text{CH}_2-\text{OCH}_3$	71.46
$\text{Ph}-\text{CH}_2-\text{OH}$	67.62
$\text{Ph}-\text{CH}_2-\text{OCH}_3$	56.18
$\text{Ph}-\text{CH}_2-\text{Cl}$	40.24
$\text{Ph}-\text{CH}_2-\text{Ph}$	35.88
$-\text{CH}_3$	18.50; 14.68

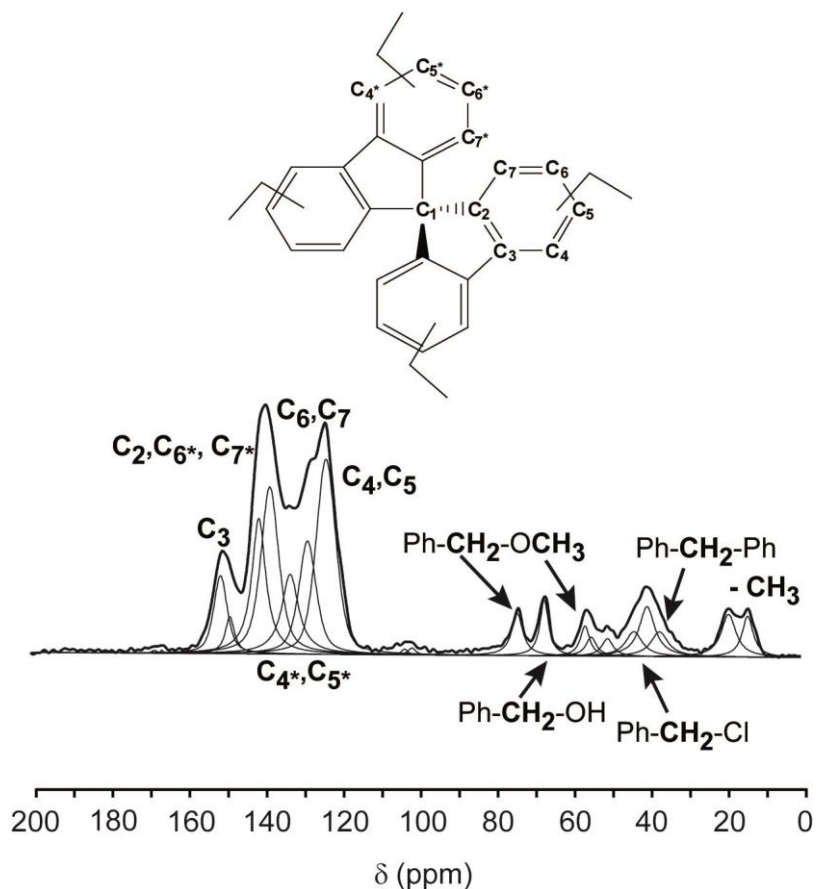


Figure S25. ^{13}C CP MAS NMR spectrum of SPBF porous polymer.

Table S6. ^{13}C Chemical shifts of SPBF porous polymer.

SPBF	
Assignment	δ (ppm)
C_3	150.68/148.25
$\text{C}_2; \text{C}_6^*; \text{C}_7^*$	140.74/137.88
$\text{C}_4^*; \text{C}_5^*$	132.66
$\text{C}_6; \text{C}_7$	128.09
$\text{C}_4; \text{C}_5$	123.08
$\text{Ph}-\text{CH}_2-\text{OCH}_3$	73.65
$\text{Ph}-\text{CH}_2-\text{OH}$	66.62
$\text{Ph}-\text{CH}_2-\text{OCH}_3$	56.05; 54.43
$\text{Ph}-\text{CH}_2-\text{Cl} / \text{Ph}-\text{CH}_2-\text{CH}_2-\text{Cl}$	43.35;
$\text{Ph}-\text{CH}_2-\text{CH}_2-\text{Cl}$	39.93
$\text{Ph}-\text{CH}_2-\text{Ph}$	36.70
$-\text{CH}_3$	18.75; 13.81

Table S7. ^{13}C Chemical shifts of TRIP porous polymer.

TRIP	
Assignment	δ (ppm)
C ₁	144.46
C ₅	136.49/131.30
C ₂ /C ₃	124.28
Ph-CH ₂ -OCH ₃	72.78
Ph-CH ₂ -OH	67.75
C ₄ ; Ph-CH ₂ -OCH ₃	55.21
Ph-CH ₂ -Cl	47.65
Ph-CH ₂ -Ph	36.32
-CH ₃	14.79

Table S8. ^{13}C Chemical shifts of HPSiO₂ porous polymer.

HPSiO ₂	
Assignment	δ (ppm)
C ₁ ; C ₄	138.36/134.21
C ₂ ; C ₃	129.04
Ph-CH ₂ -OCH ₃	73.37
Ph-CH ₂ -OCH ₃	56.58
Ph-CH ₂ -Ph	36.60
-CH ₃	17.72/14.11

Table S9. ^{13}C Chemical shifts of STIL porous polymer.

STIL	
Assignment	δ (ppm)
C _{1a} ; C _{2a*} ; C _{4a*}	138.41
C ₁ ; C ₃ ; C _{2a} ; C _{4a}	128.20
Ph-CH ₂ -OCH ₃	73.61
Ph-CH ₂ -OH	66.66
Ph-CH ₂ -OCH ₃	56.38
Ph-CH ₂ -Cl	41.81
Ph-CH ₂ -Ph	36.46
-CH ₃	18.32/14.55

Table S10. ^{13}C Chemical shifts of HPSiSi porous polymer.

HPSiSi	
Assignment	δ (ppm)
C ₁ ; C ₄	138.16/134.41
C ₂ ; C ₃	129.15
Ph-CH ₂ -OCH ₃	73.30
Ph-CH ₂ -OCH ₃	57.03; 55.40
Ph-CH ₂ -Ph	36.70
-CH ₃	190.07/16.67/13.54

Table S11. ^{13}C Chemical shifts of HPPh porous polymer.

HPB	
Assignment	δ (ppm)
C ₁ ; C ₂ ; C ₅	140.28/137.25
C ₃	131.72
C ₄	126.40
Ph-CH ₂ -OCH ₃	72.96
Ph-CH ₂ -OCH ₃	55.63
Ph-CH ₂ -Cl / Ph-CH ₂ -CH ₂ -Cl	43.95
Ph-CH ₂ -CH ₂ -Cl	40.74
Ph-CH ₂ -Ph	34.93
-CH ₃	17.32; 13.86

Table S12. ^{13}C Chemical shifts of RUB porous polymer.

RUB	
Assignment	δ (ppm)
C ₁	153.05
C ₂	140.17
C ₃ ; C ₄ ; C ₅ ; C _{7*}	135.63
C ₆ ; C ₇ ; C ₈ ; C ₉	127.21
Ph-CH ₂ -OCH ₃	73.44
Ph-CH ₂ -OH	61.11
Ph-CH ₂ -OCH ₃	55.99
Ph-CH ₂ -Cl	43.02
Ph-CH ₂ -Ph	37.94
-CH ₃	17.99

Table S13. ^{13}C chemical shift of porous polymers from Yamamoto-type reaction.

CBZ1	
Assignment	δ (ppm)
C ₁ , C ₉ , C ₂	140.90/136.56
C ₅ , C ₆ , C ₇	127.52; 124.79;
C ₈	119.44
C ₁₀	109.40

CBZ2	
Assignment	δ (ppm)
C ₁ , C ₄ , C ₉ , C ₂	140.43/136.98
C ₃ , C ₅ , C ₆ , C ₇	127.14/124.66
C ₈	119.60
C ₁₀	109.70

PAF1	
Assignment	δ (ppm)
C ₅	146.31
C ₂	139.79
C ₃	131.27
C ₄	125.40
C ₁	64.49

PAFPOR	
Assignment	δ (ppm)
C ₅	145.90
C ₁ , C ₄ , C ₆	140.80
C ₂	139.79
C ₂ , C ₃	130.90
C ₃	131.27
C ₄	126.00
C ₇	124.95
C ₅	118.04
C ₁	64.70

PORP	
Assignment	δ (ppm)
C ₁ , C ₄ , C ₆	140.80
C ₂ , C ₃	131.17
C ₇	124.95
C ₅	118.01

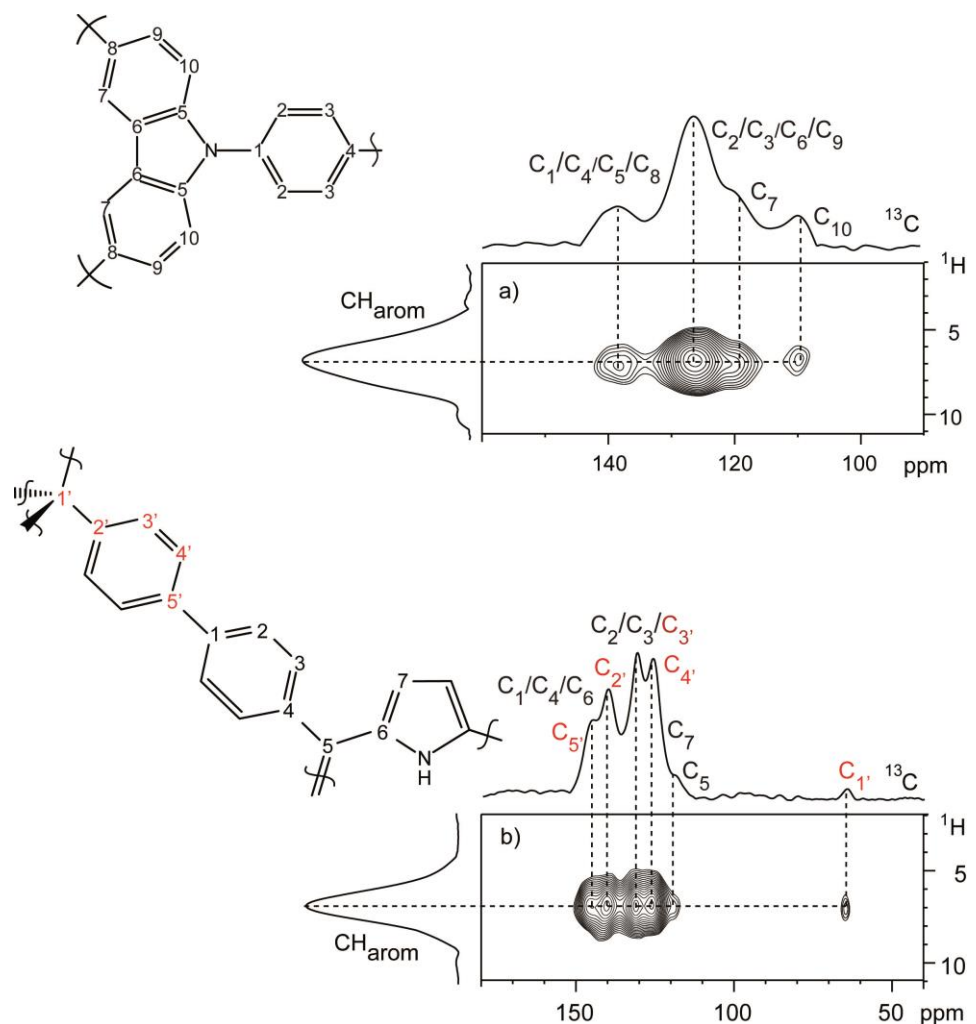


Figure S26. 2D ^1H - ^{13}C HETCOR NMR spectra of CBZ2 and PORP porous compounds.

5. N₂ Adsorption Isotherms

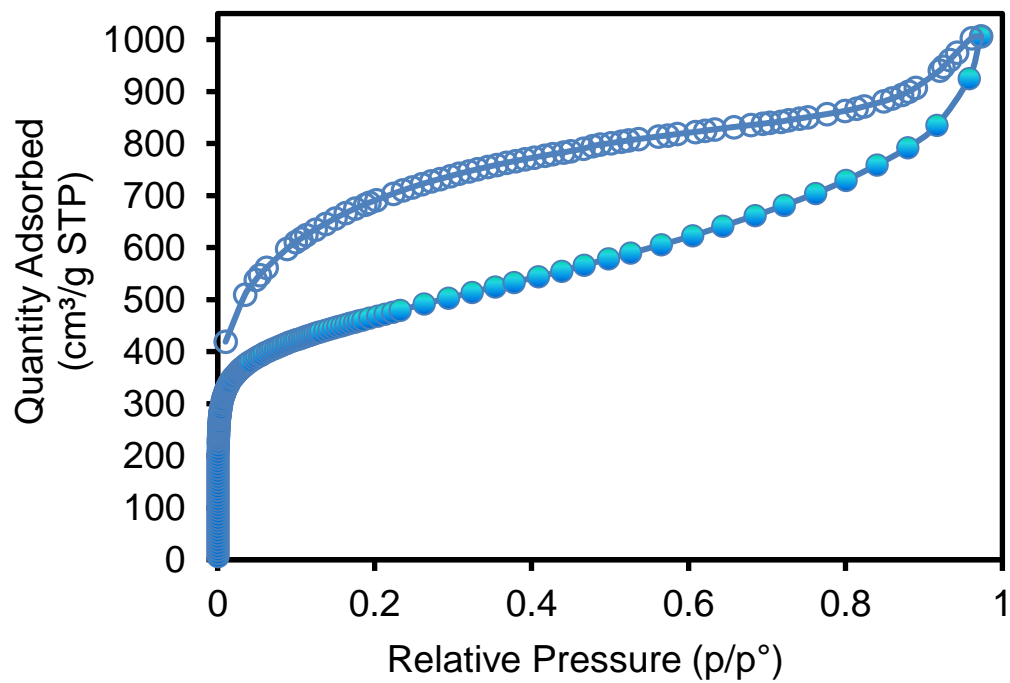


Figura S27. N₂ adsorption isotherm of CBZ2 at 77 K.

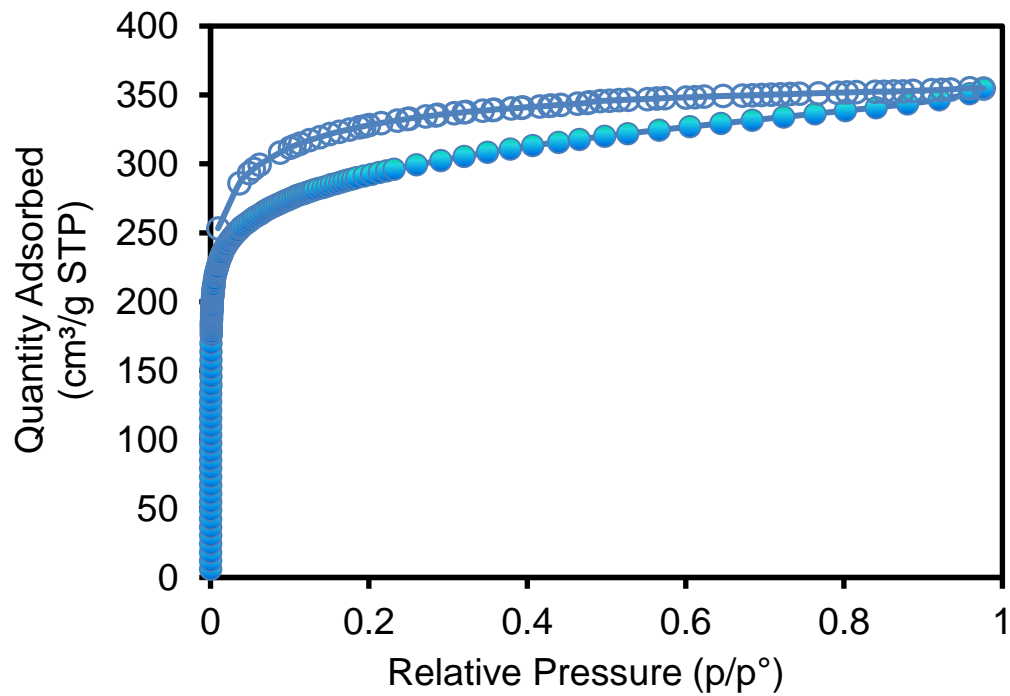


Figure S28. N₂ adsorption isotherm of CBZCH₂ at 77 K.

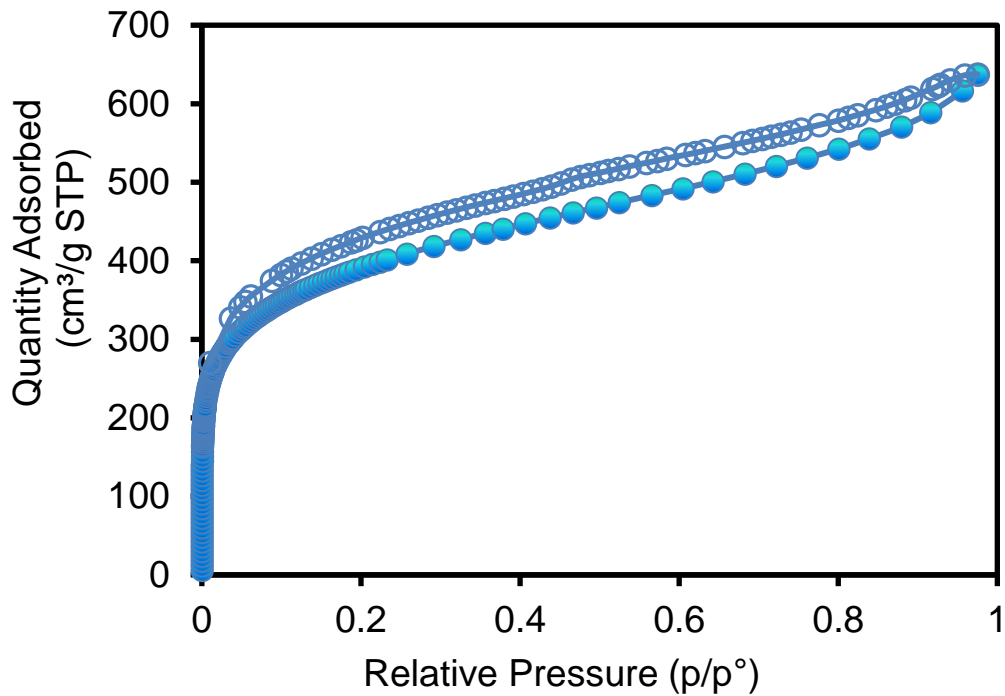


Figure S29. N₂ adsorption isotherm of SPBF at 77 K.

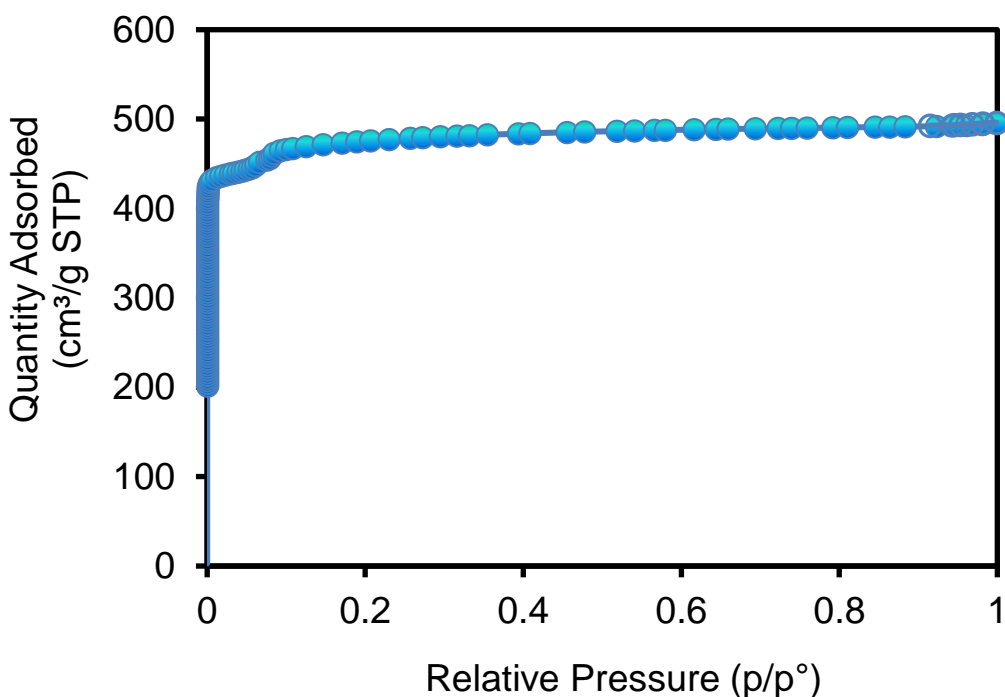


Figure S30. N₂ adsorption isotherm of HKUST-1 at 77 K (BET surface area = 1834 m²/g, Langmuir surface area = 2157 m²/g, V_p=0.77 cm³/g).

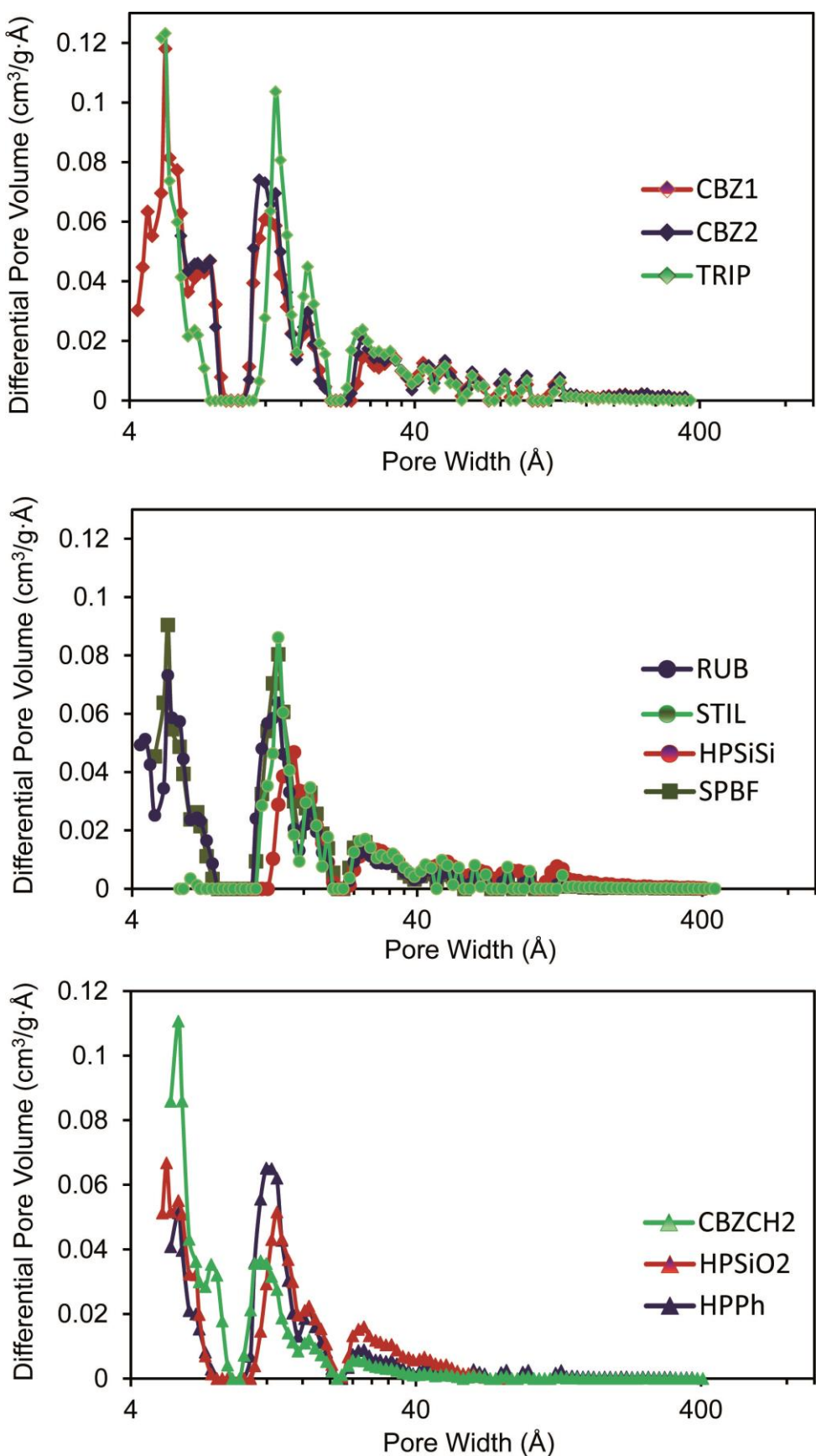


Figure S31. Pore size distribution as calculated by NLDFT method and carbon slit pore model.

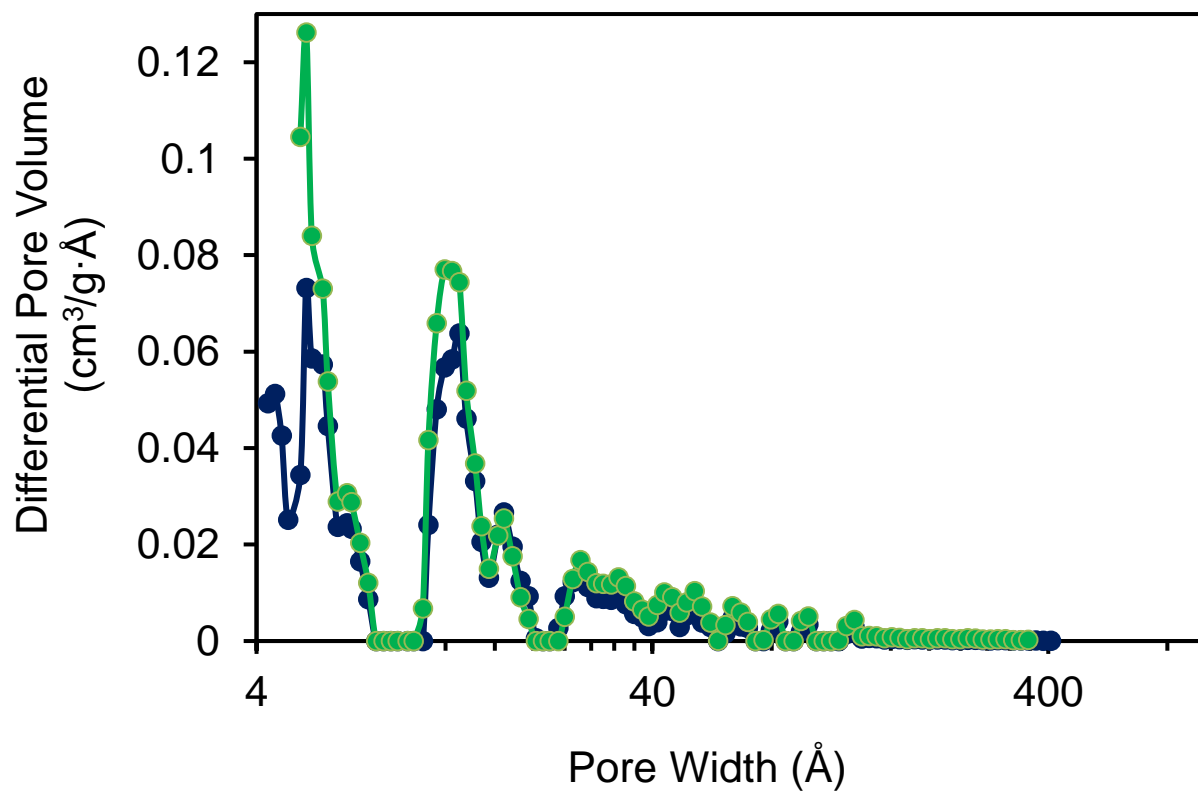
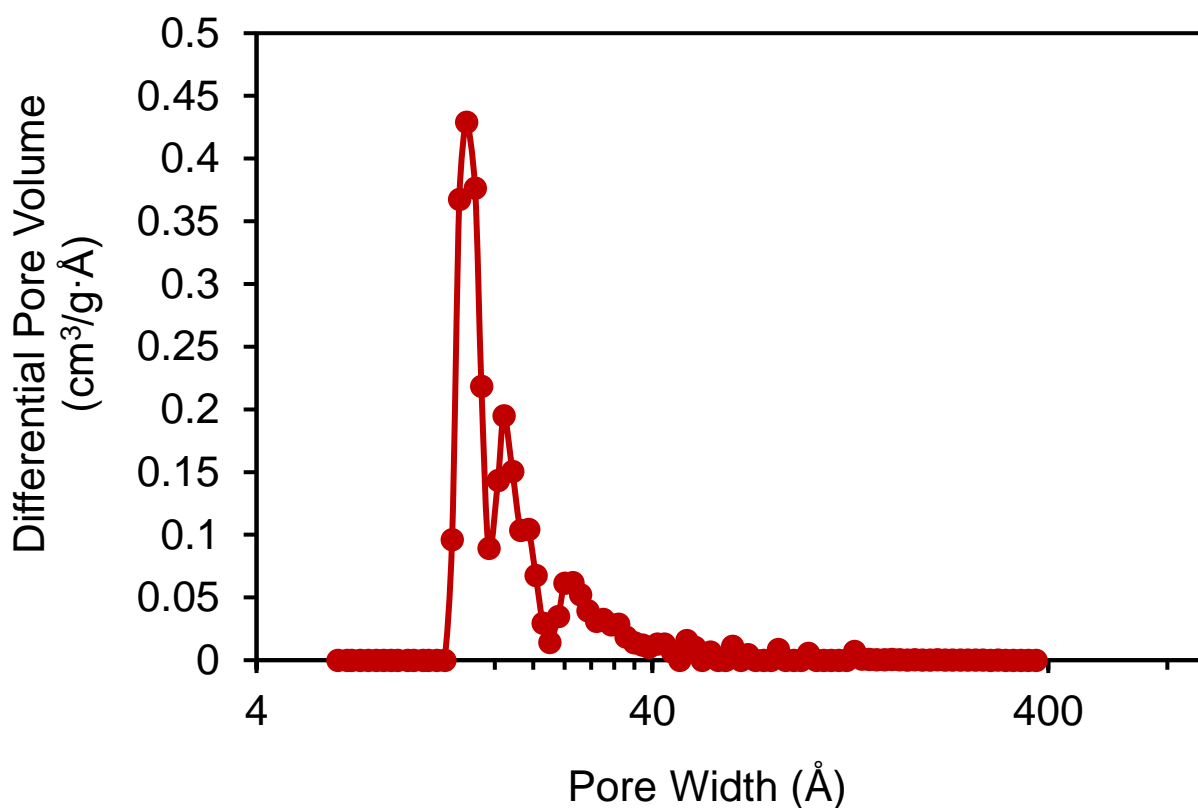


Figure S32. Pore size distribution of PAF1 (above) and PAFPORP and PORP (below) as calculated by NLDFT method and carbon slit pore geometry. PAF1 (red labels), PAFPORP (blue labels) and PORP (green labels).

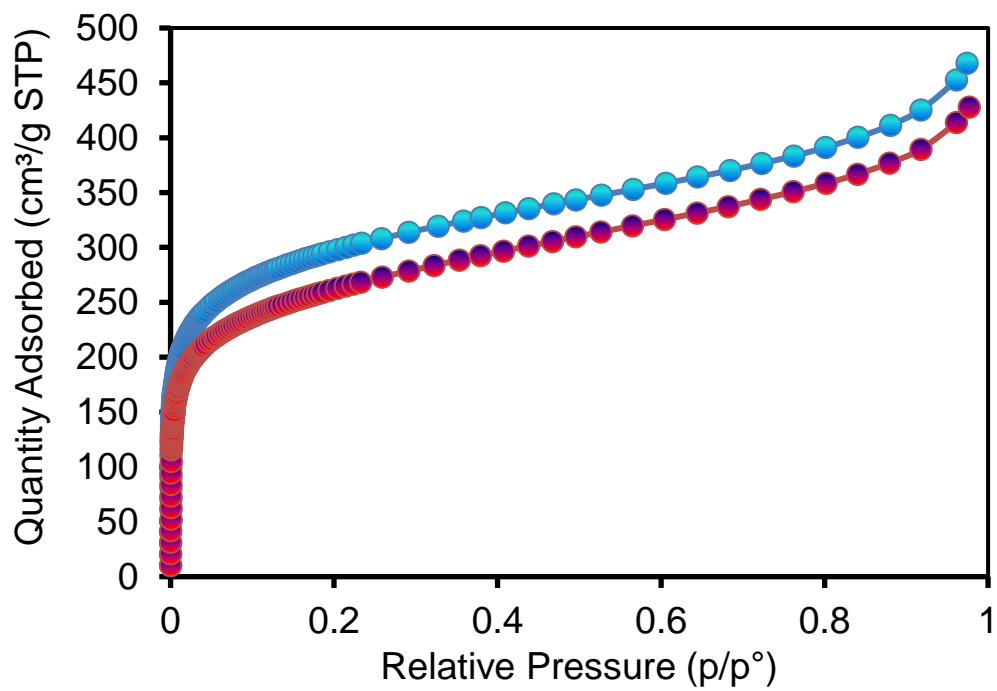


Figure S33. N₂ adsorption isotherms of HPPh before (blue) and after (red) pressure treatment at 9000 psi.

6. CH₄ Adsorption Isotherms and Isosteric Heat of Adsorption

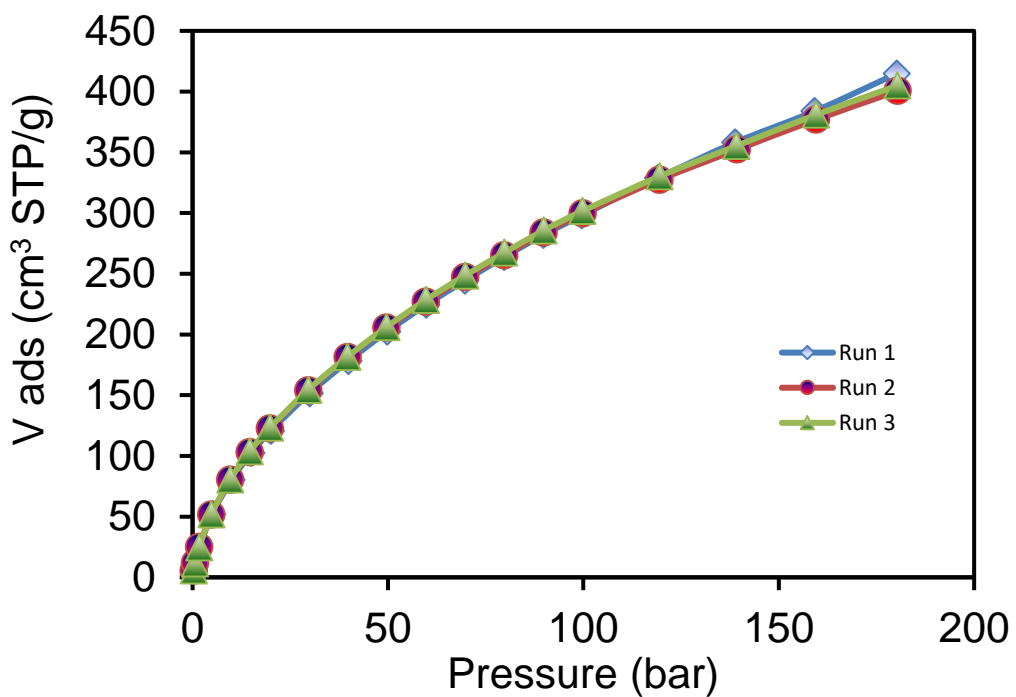


Figure S34. CH₄ adsorption isotherms of TRIP at 298 K showing the reproducibility of the adsorption process.

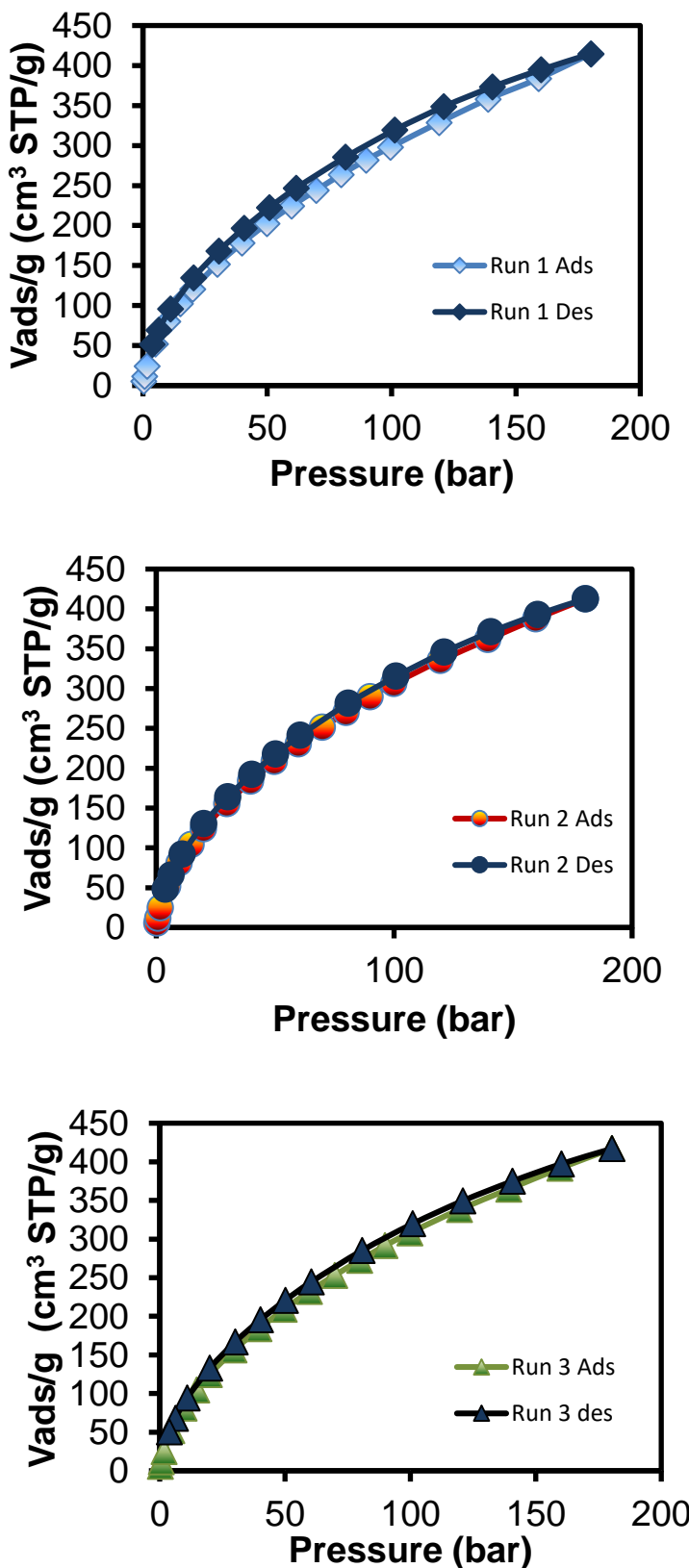


Figure S35. CH_4 adsorption/desorption isotherms of TRIP at 298 K, showing the reversibility of the process.

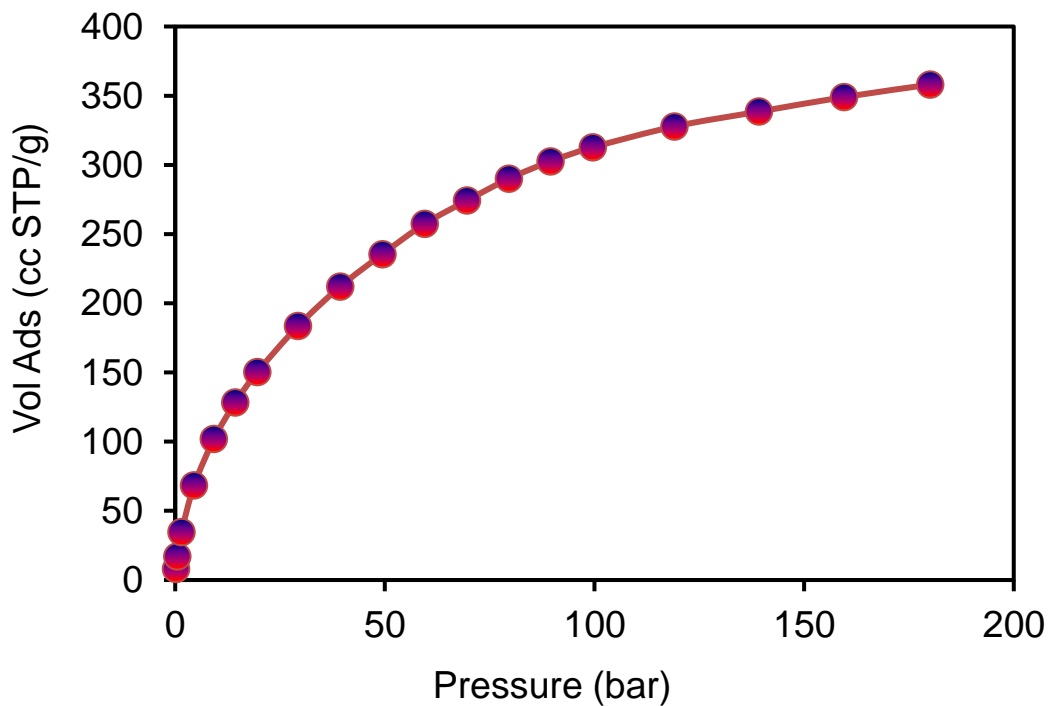


Figure S36. CH₄ adsorption isotherm of TRIP at 273 K.

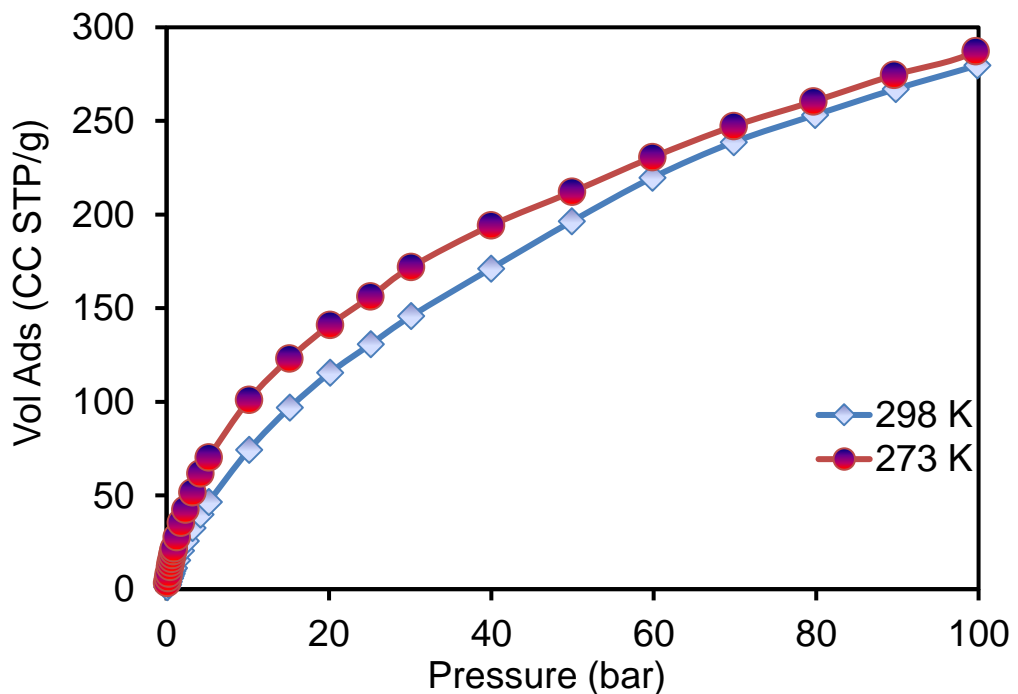


Figure S37. CH₄ adsorption isotherm of PORP at 273 K (red) and 298 K (light blue).

Table S14. CH₄ adsorption values at 35, 65, 100, 180 bar.

Sample name	Quantity adsorbed (cm ³ /cm ³ STP)				Quantity adsorbed (cm ³ /g STP)			
	Pressure 35 bar	Pressure 65 bar	Pressure 100 bar	Pressure 180 bar	Pressure 35 bar	Pressure 65 bar	Pressure 100 bar	Pressure 180 bar
PAF-1	94	145	187	266	317	487	643	916
PAFPORP	88	125	155		251	358	443	
CBZ1	94	126	159	218	188	252	318	436
CBZ2	93	127	164	226	186	255	328	452
SPBF	84	117	144	173	140	195	240	289
TRIP	94	112	165	220	171	204	300	400
PORP	87	127	154		158	230	280	
CBZCH2	88	106	120	134	110	200	228	167
RUB	85	115	143	167	147	198	247	289
HPPh	76	102	125	160	115	155	189	242
STIL	79	110	140	196	129	180	230	322
HPSiSi	72	102	132	182	131	185	240	332
HPSiO2	86	117	147	193	102	139	175	230

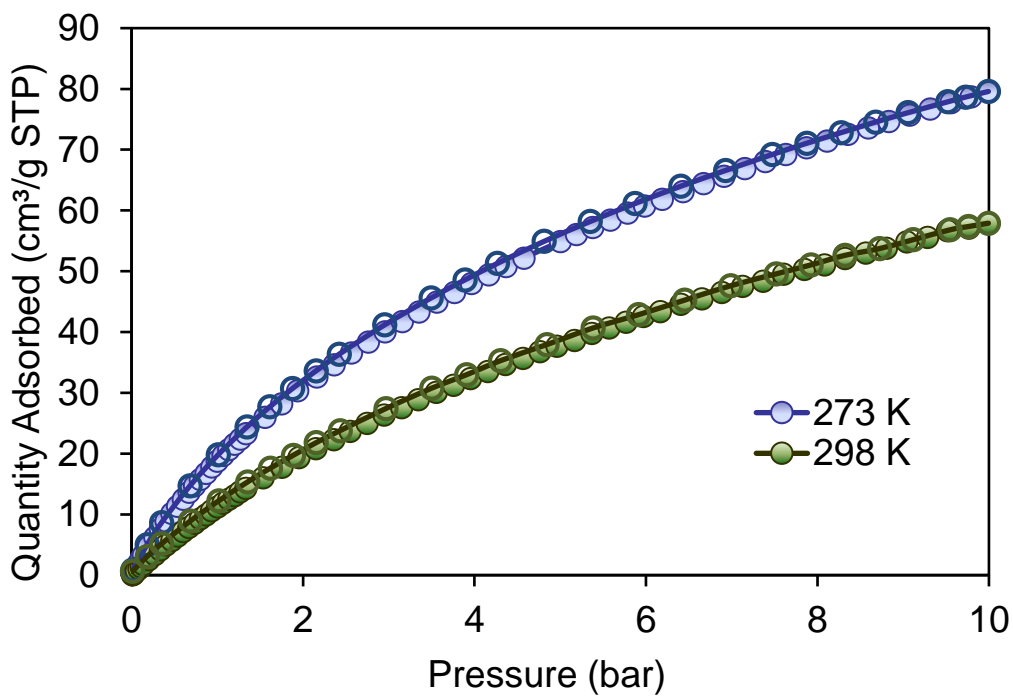


Figure S38. CH₄ adsorption isotherm of PORP at 273 K (blue) and 298 K (green) to 10 bar.

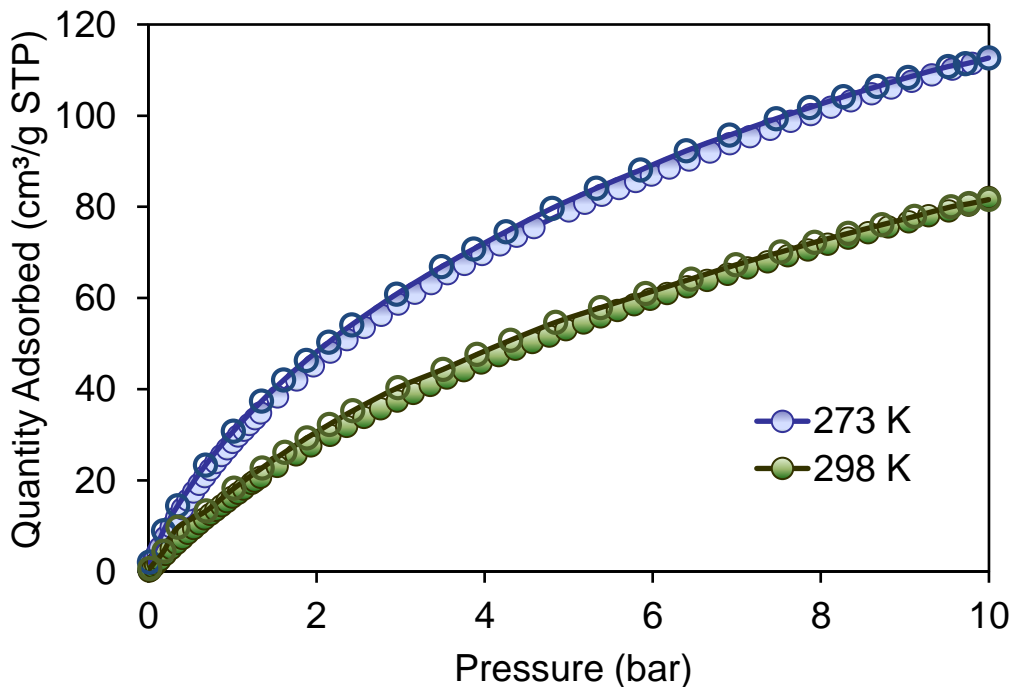


Figure S39. CH₄ adsorption isotherm of RUB at 273 K (blue) and 298 K (green) to 10 bar.

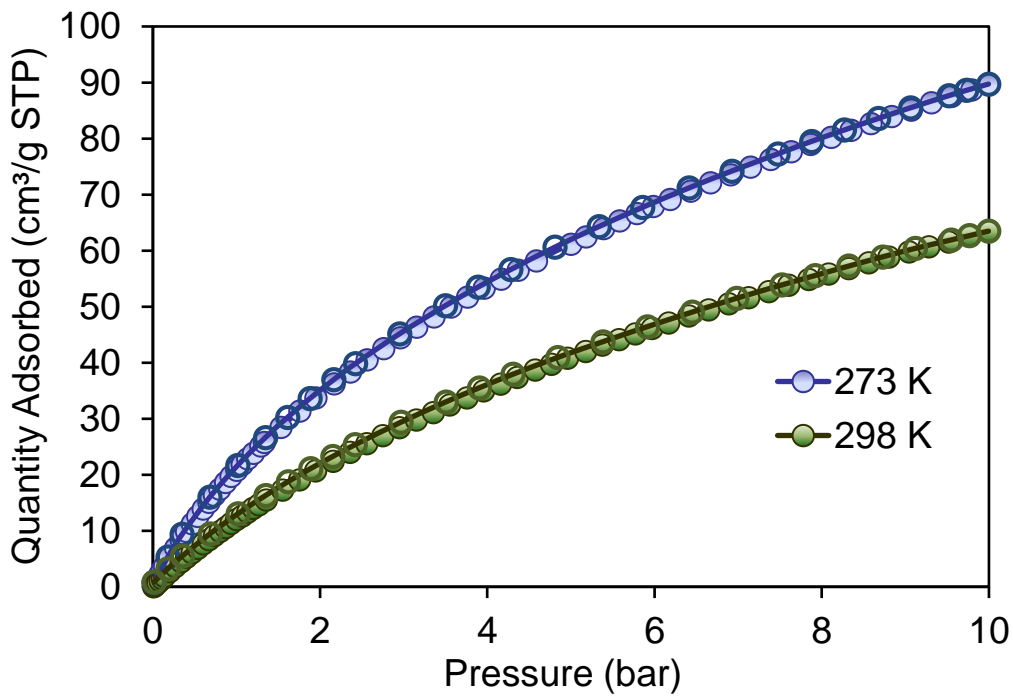


Figure S40. CH₄ adsorption isotherm of SPBF at 273 K (blue) and 298 K (green) to 10 bar.

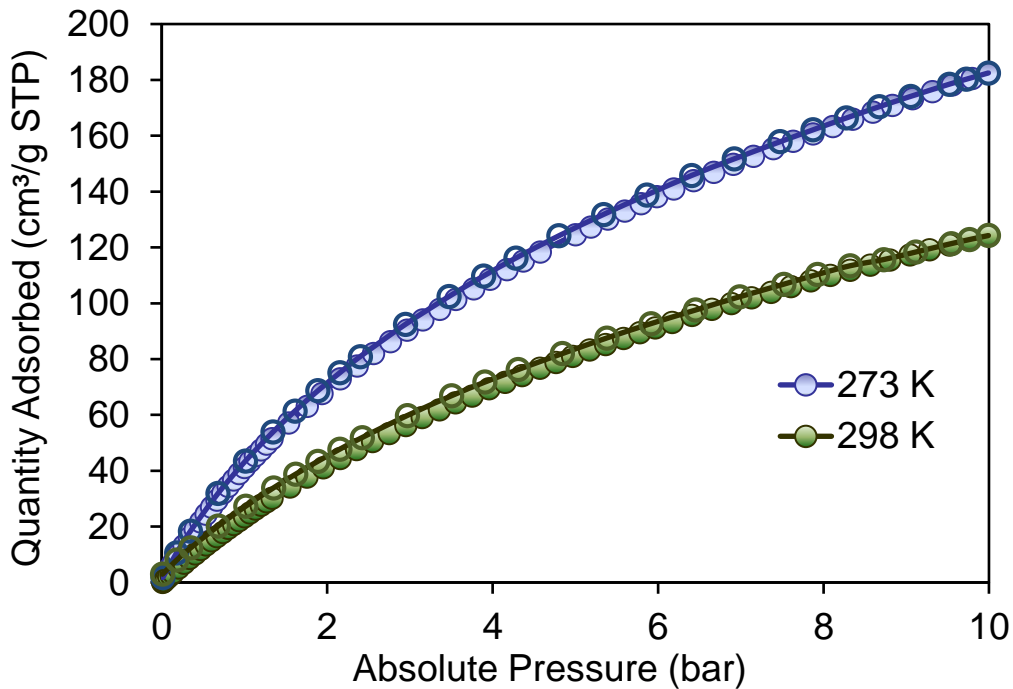


Figure S41. CH₄ adsorption isotherm of CBZ1 at 273 K (blue) and 298 K (green) to 10 bar.

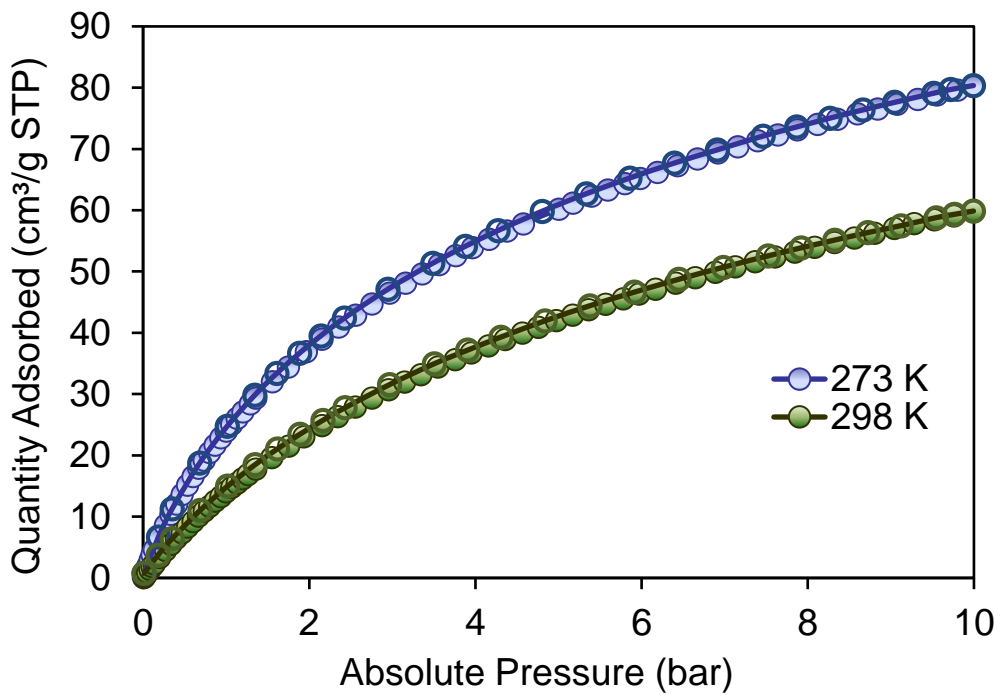


Figure S42. CH_4 adsorption isotherm of CBZCH₂ at 273 K (blue) and 298 K (green) to 10 bar.

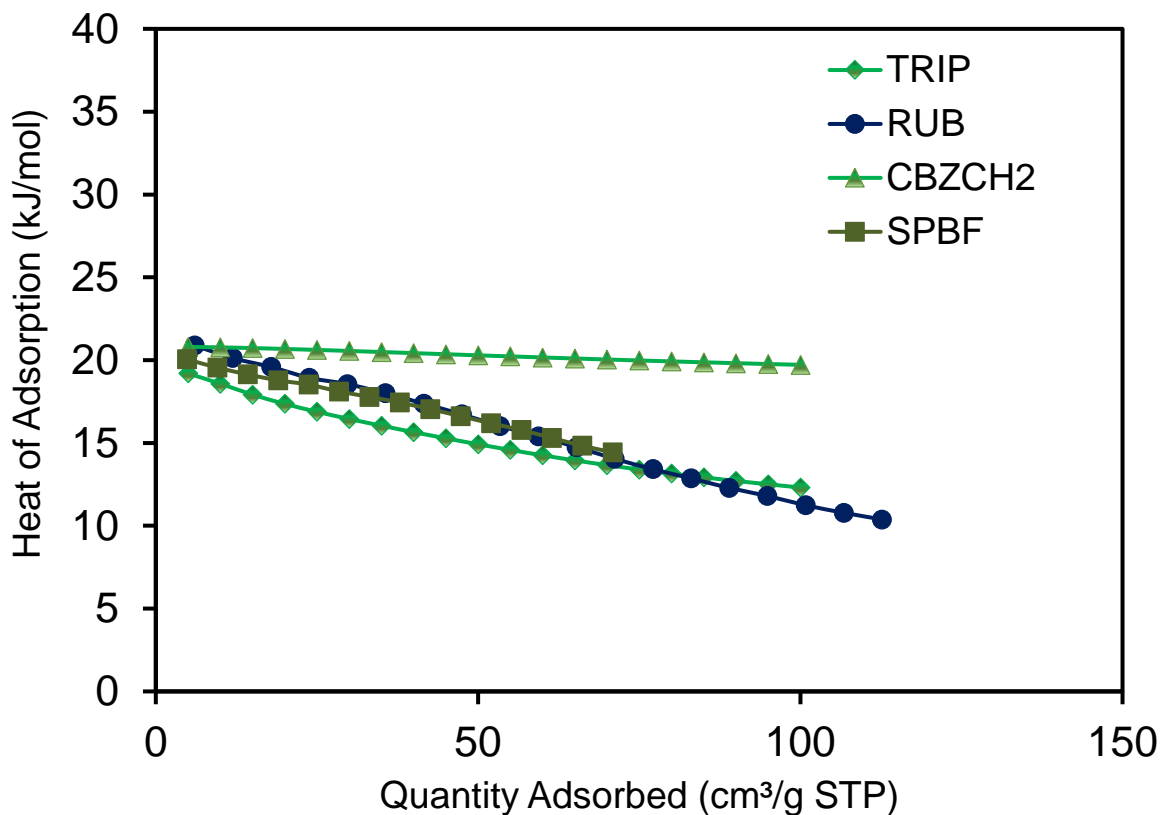
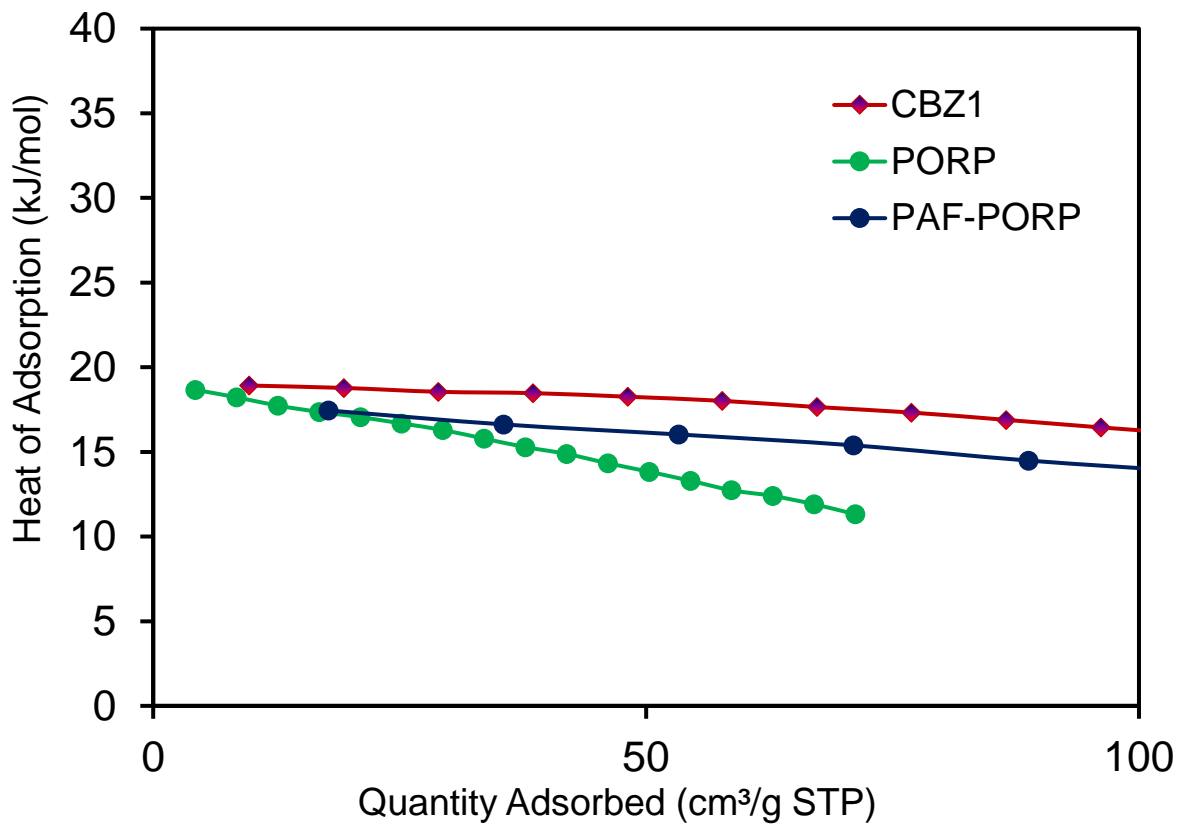


Figure S43. CH_4 isosteric heat of adsorption.

7. CO₂ Adsorption Isotherms and Isosteric Heat of Adsorption

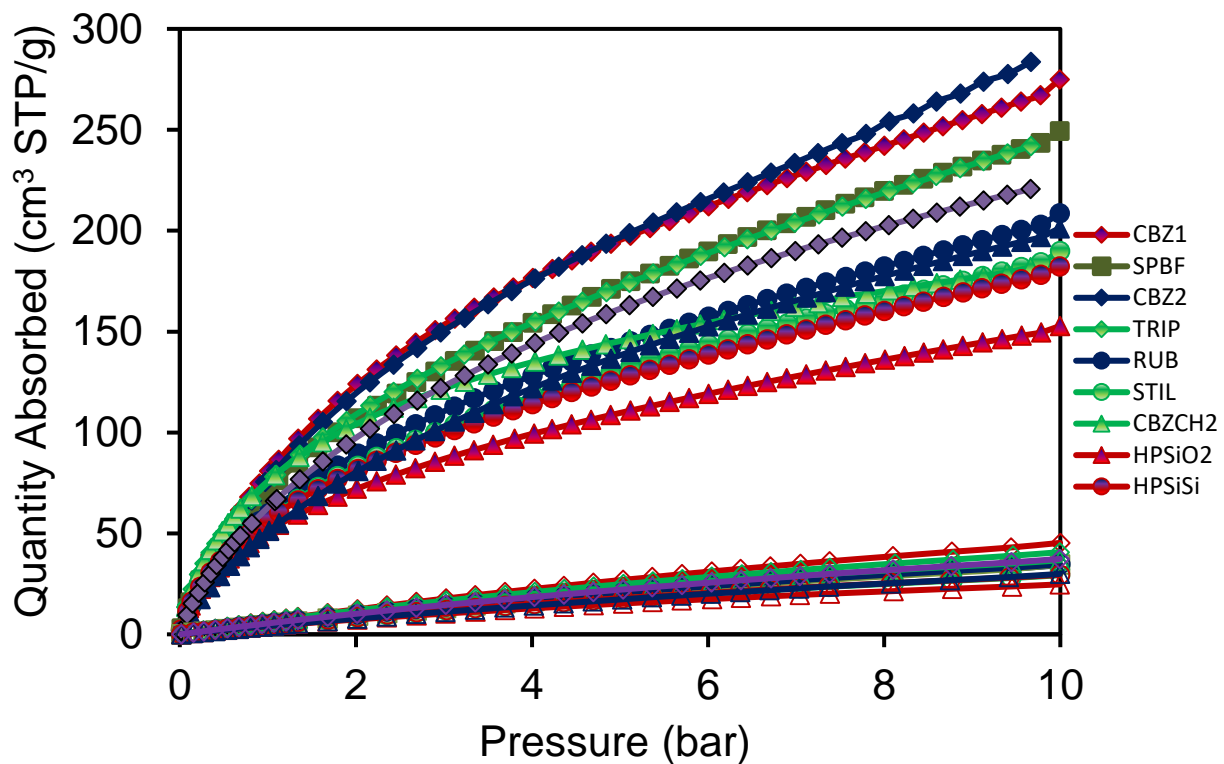


Figure S44. CO₂ (filled labels) and N₂ (empty labels) adsorption isotherm of porous polymers at 273 K and up to 10 bar.

Table S15. CO₂ adsorption values at 10 bar. Q indicates the CO₂ adsorbed amount.

Sample	Q (cm³/g)	Q (cm³/g)	Q_{273K}/Q_{298K}
	273K	298K	
PAF-1	850.7	266.7	3.2
PAFPORP	542.7	247.5	2.2
CBZ1	274.9	183.1	1.5
CBZ2	283.6	174.0	1.6
SPBF	249.3	163.2	1.5
TRIP	241.9	161.5	1.5
PORP	220.7	150.4	1.5
CBZCH2	181.9	134.4	1.4
RUB	208.6	132.5	1.6
HPPh	201.2	127.5	1.6
STIL	189.8	122.7	1.5
HPSiSi	182.3	118.3	1.5
HPSiO2	152.7	101.8	1.5

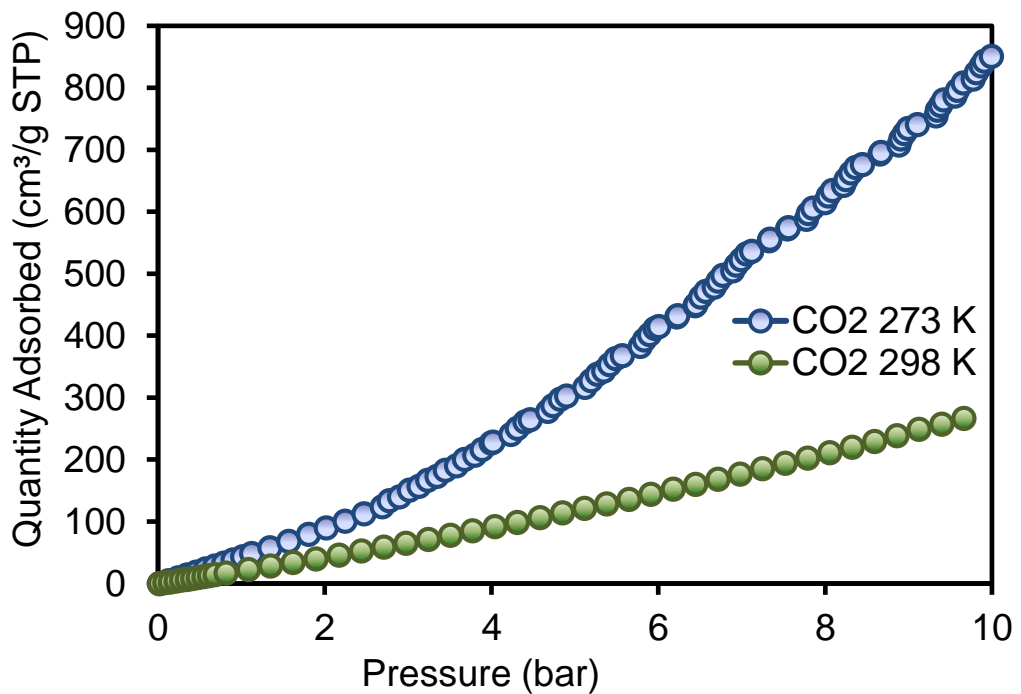


Figure S45. CO₂ adsorption isotherm of PAF1 at 273 K (blue) and 298 K (green) to 10 bar.

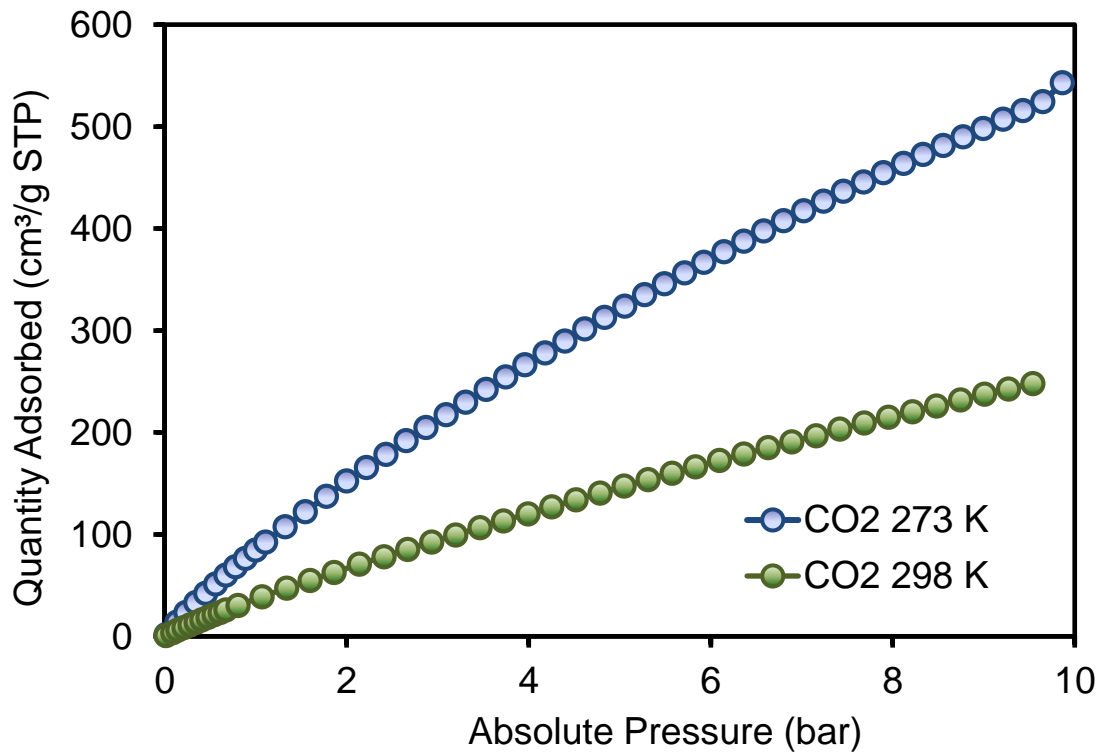


Figure S46. CO₂ adsorption isotherm of PAFPORP at 273 K (blue) and 298 K (green) to 10 bar.

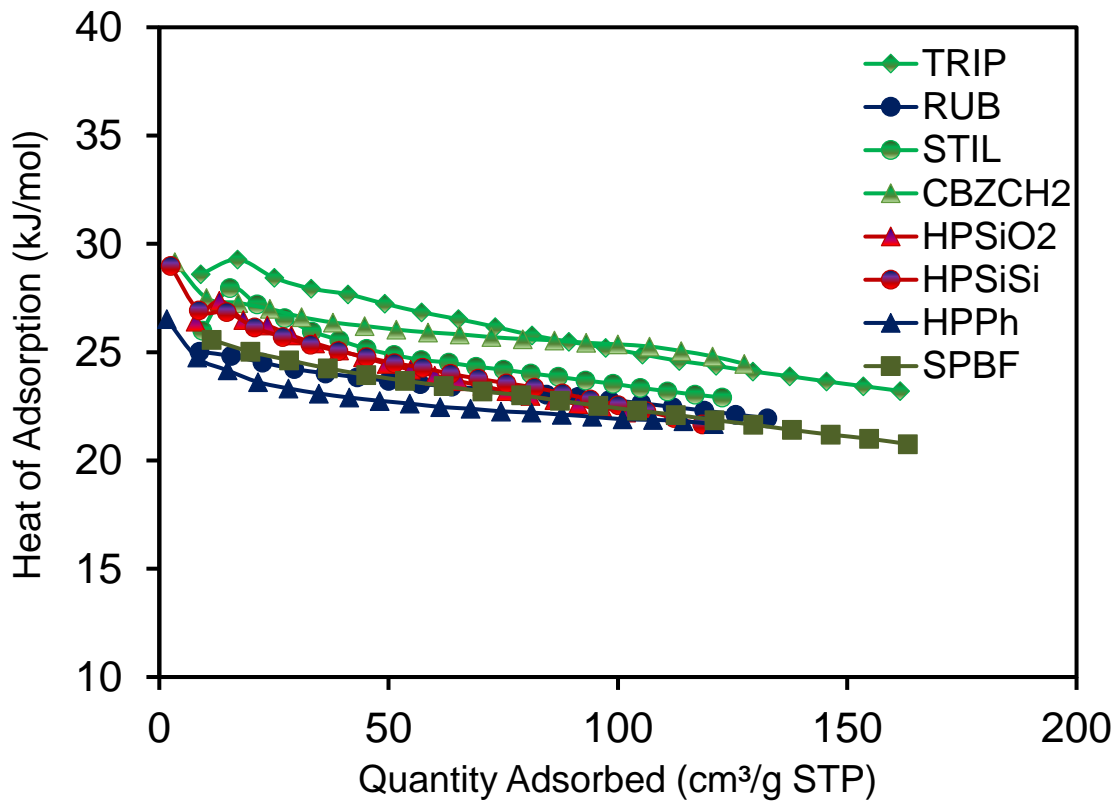
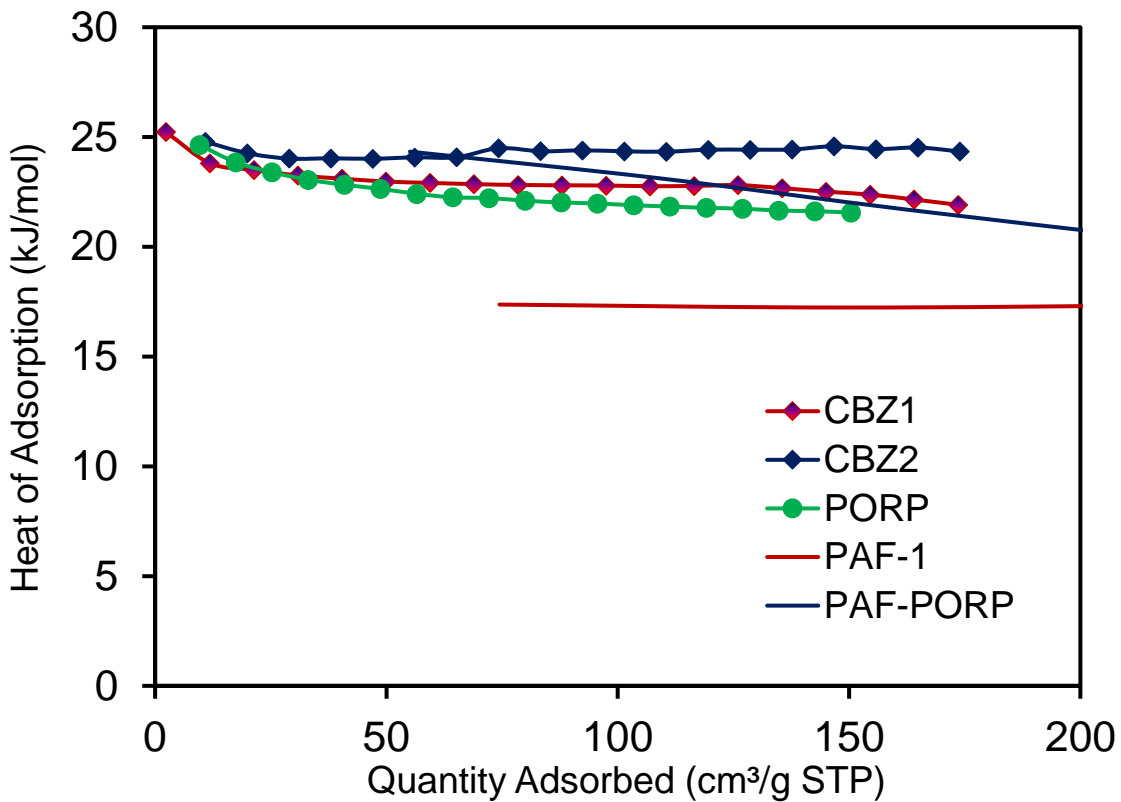


Figure S47. Isosteric heat of adsorption of CO_2 .

8. CO₂/N₂ Selectivity

The selectivity of CO₂-N₂ binary mixture of 15:85 was determined from the single-component isotherms using ideal adsorbed solution theory (IAST), which has been successfully used to calculate gas mixture separation by microporous materials.

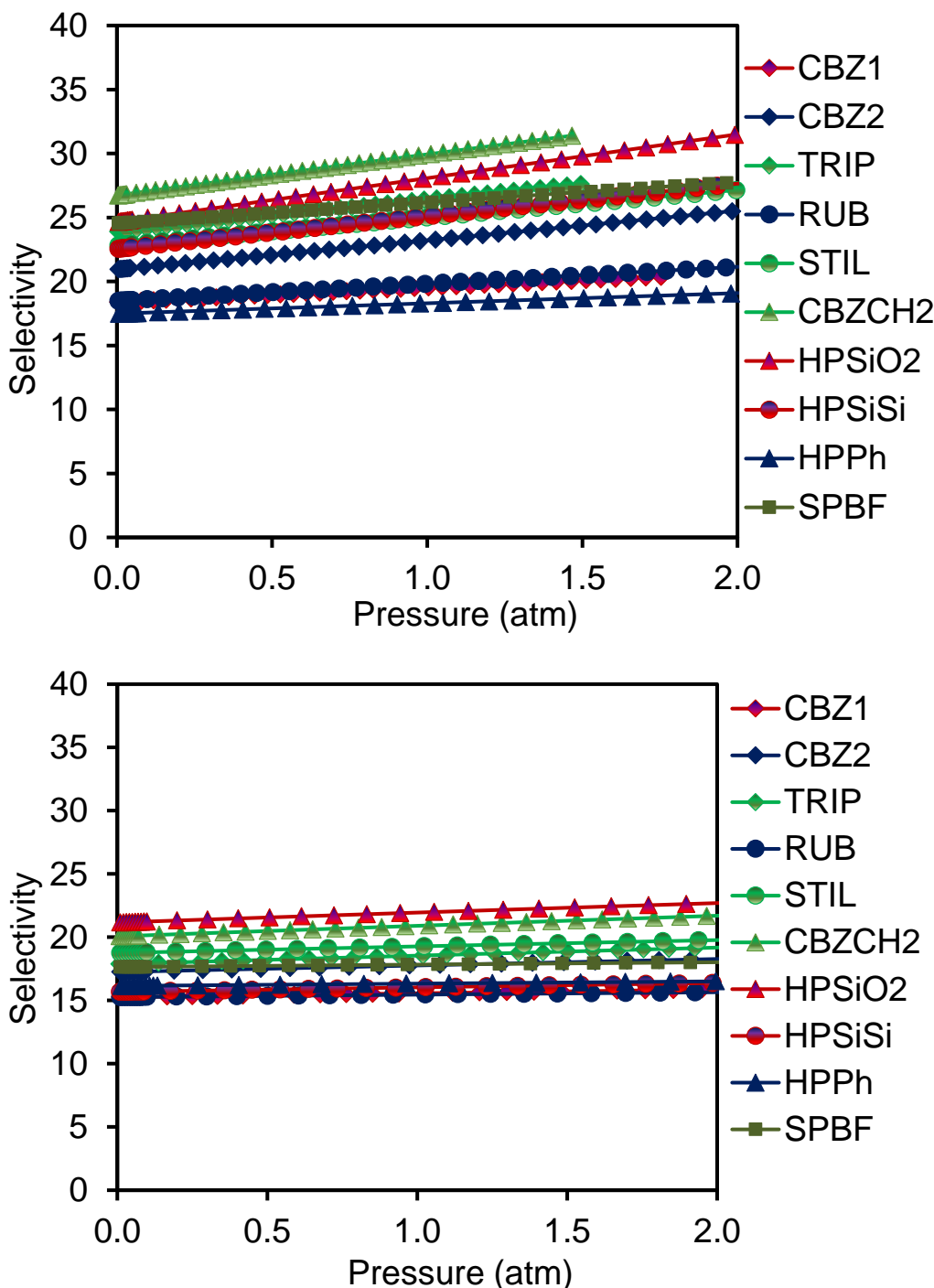


Figure S48. CO₂/N₂ selectivity for binary gas mixture with a 15:85 molar composition at 273K (above) and 298 K (below).

9. Powder X-ray diffraction PXRD

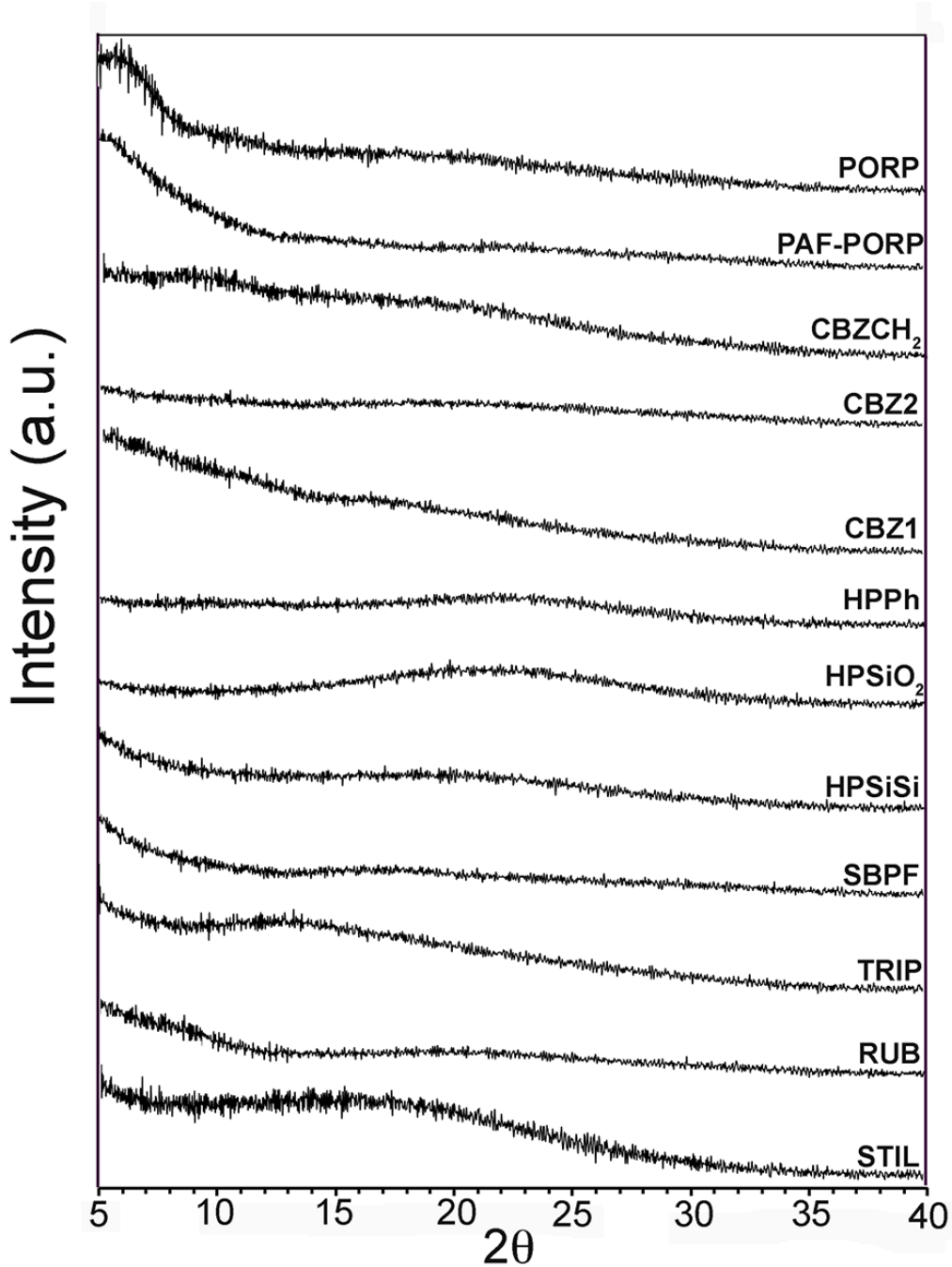


Figure S49. Powder X-ray diffraction patterns of the porous polymers.